Chapter 4
Sawtooth Instability

Ian T. Chapman

Abstract Sawtooth oscillation results in a periodic relaxation of the tokamak core plasma. These periodic oscillations consist of a quiescent period, during which the density and temperature increase, followed by a rapid collapse in the core pressure, which is often preceded by the growth of a helical magnetic perturbation. The period between these rapid sawtooth collapses is expected to increase in the presence of alpha particles in burning fusion plasmas. However, long sawtooth periods have been observed to increase the likelihood of triggering neoclassical tearing modes (see chapter 8) at lower plasma pressures; these instabilities in turn can then significantly degrade the plasma confinement. Consequently, recent efforts have focussed on developing methods to deliberately trigger short sawtooth periods to avoid seeding NTMs while retaining the benefits of core impurity expulsion. The main sawtooth control tools involve driving localised currents to change the safety factor profile or tailoring the fast ion distribution.

4.1 Introduction

Sawtooth oscillations are periodic relaxations of the core plasma density and temperature [1–3]. These periodic redistributions of the plasma surrounding the magnetic axis were first observed in 1974 [4] and are commonplace in every tokamak. A typical sawtooth cycle is illustrated in Fig. 4.1, showing the three phases: (i) the sawtooth ramp phase during which the plasma density and temperature increase in time; (ii) the precursor phase, during which a helical magnetic perturbation grows until (iii) the fast collapse phase, when the density and temperature in the core drop rapidly. Sometimes magnetic fluctuations are also observed after the sawtooth crash (post-cursors) [5] or even during the ramp phase [6]. When a sawtooth crash occurs, hot electrons transport rapidly to a cooler region of plasma, such that the electron

I.T. Chapman (✉)
CCFE, Culham Science Centre, Abingdon, Oxfordshire OX14 3DB, UK
e-mail: ian.chapman@ccfe.ac.uk

V. Igochine (ed.), *Active Control of Magneto-hydrodynamic Instabilities in Hot Plasmas*, Springer Series on Atomic, Optical, and Plasma Physics 83,
DOI 10.1007/978-3-662-44222-7_4

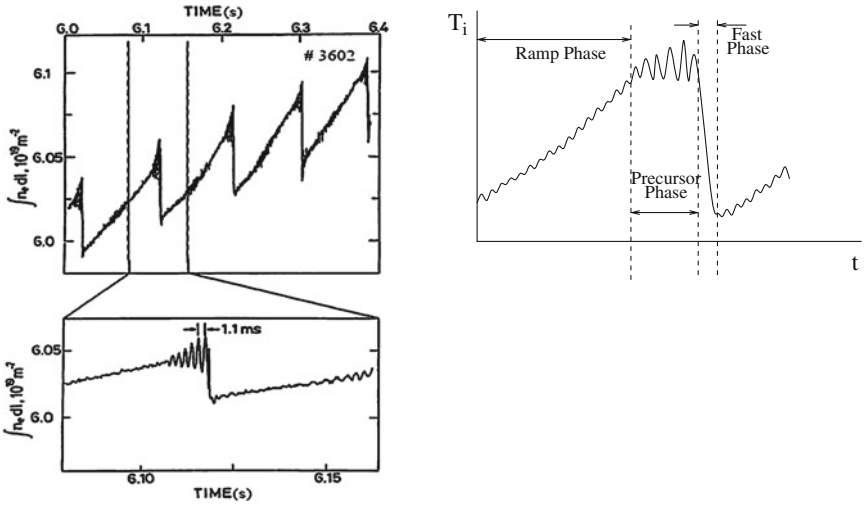

Fig. 4.1 The line-integrated electron density of a JET plasma exhibiting sawtooth oscillations. The sawteeth consist of a ramp phase, then a precursor oscillation followed by the fast collapse

temperature profile is flattened. This rapid drop in the core temperature is accompanied by heating of the edge plasma. The temperature remains constant at the *inversion radius*. Two-dimensional imaging of the collective behaviour during a sawtooth crash [7, 8] shows clearly that the hot plasma core is expelled through a poloidally localised point as magnetic reconnection occurs, as illustrated in Fig. 4.2.

In order to control sawteeth, it is most important to understand the second phase in the cycle—the trigger of the instability growth—which is discussed in detail in Sect. 4.2. Experiments have shown (see [1] and references therein) that the precursor oscillation has the topology of the $n = m = 1$ internal kink mode—a fundamental magnetohydrodynamic (MHD) oscillation of the form $\xi \sim \exp(im\theta - in\phi)$ where m and n are the poloidal and toroidal mode number respectively, ξ is the perturbation to the plasma and θ and ϕ are the poloidal and toroidal angles. The ideal internal kink displacement, which is manifest as the precursor oscillation, takes the form of a tilt and a shift of the core plasma (although it should be noted that tokamak plasmas do sometimes experience precursorless sawteeth [9]). The behaviour of the kink mode can be adequately described by MHD. However, the dynamics of energetic particles (for instance born due to Ion Cyclotron Resonance Heating (ICRH) or Neutral Beam Injection (NBI), or α particles from fusion reactions), which affect the stability of the kink mode, must be treated kinetically and the various stabilising and destabilising terms assessed using the energy principle. In essence this says that if a physically allowable perturbation lowers the potential energy of the plasma, then the wave is unstable [2].

Small sawteeth which have an inversion radius smaller than 40 % of the minor radius and a temperature drop of the order of a fraction of a keV can be tolerated by the plasma [10]. Indeed, such small sawteeth can help to prevent the accumulation of

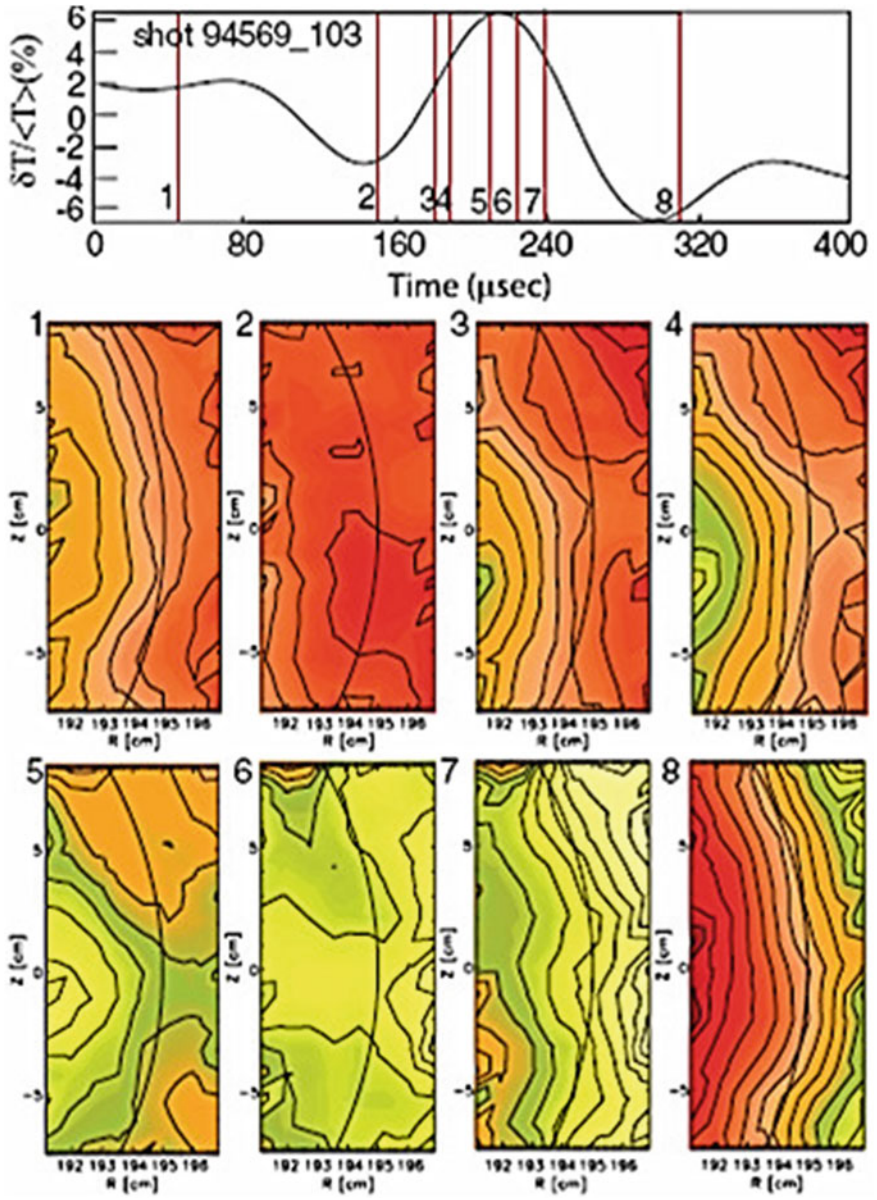

Fig. 4.2 2D images of the sawtooth crash from electron cyclotron emission imaging at the low-field side mid-plane on TEXTOR. As the hot spot swells (shown in *frames 3* and *4*) a sharp temperature point is growing and crosses beyond the inversion radius (marked by the *black arc*). Eventually, the temperature point leads to the reconnection. Initially, it forms an X-point in the poloidal plane (*frame 5*), and heat starts to flow to the outside through a small opening. The initial heat flow is highly collective, and the opening increases up to 15 cm. At the end, the heat accumulates outside the inversion radius, and the poloidal symmetry is recovered. Reprinted figure with permission from Park et al. [7]. Copyright 2006 by the American Physical Society

impurities in the core plasma, such as the helium ash resultant from fusion reactions [11]. Conversely, long period sawteeth with an inversion radius approaching half of the minor radius and a large temperature perturbation can couple to other more deleterious instabilities. It has been shown that plasmas with long period sawteeth are more susceptible to Edge Localised Modes (ELMs) [12] and Neo-classical Tearing Modes (NTMs) [13–21] (see Fig. 4.3). NTMs are resistive tearing modes which are sustained by a perturbation to the bootstrap current (a current caused by pressure gradients in the plasma) [22–26]. Unlike sawteeth, NTMs are long-living instabilities and their presence degrades both the plasma energy and the angular momentum [18] and can even lead to terminations. The NTM is a metastable mode which requires a *seed* perturbation in order to be driven unstable and grow [22], except at very high plasma pressure where the linear tearing stability index Δ' can become large and positive as it approaches a pole discontinuity [27]. Various effects have been proposed to prevent NTM growth for small island widths, namely (i) incomplete pressure flattening which occurs when the connection length is long compared to the island width [28], (ii) ion polarisation currents arising due to finite orbit width $E \times B$ drifts occurring for ions and electrons across the island region [29, 30], which act to replace the missing bootstrap current, and (iii) curvature effects [31, 32]. Many theories have been proposed to explain how the sawtooth crash triggers the NTM, including magnetic coupling [33], nonlinear 'three-wave' coupling [34], changes in the classical tearing stability due to current redistribution inside $q = 1$ [35–37] or changes in the rotation profile resulting in a reversal of the ion polarisation current [19] in the modified Rutherford equation governing NTM

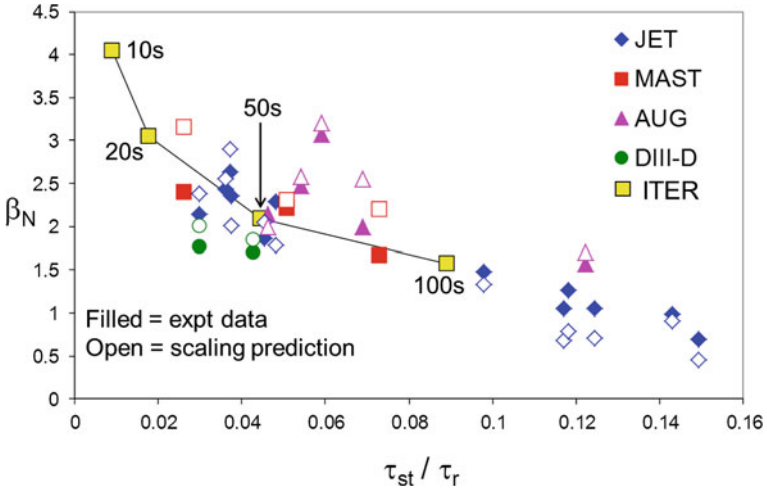

Fig. 4.3 β_N at the NTM onset with respect to the sawtooth period normalised to the resistive diffusion time for ITER-like shape, $q = 1$ radius and injected power normalised in a range just above the P_{LH} threshold. For comparison, ITER baseline scenario is indicated with sawtooth period ranging from 10 to 100 s. Reproduced with permission from "Power requirements for electron cyclotron current drive and ion cyclotron resonance heating for sawtooth control in ITER" [185]

stability [25]. Figure 4.3 shows how the critical β_N at which an NTM is triggered varies with respect to the sawtooth period normalised to the resistive diffusion time. It is evident that as the sawtooth period lengthens, the NTMs are triggered at lower β_N, hence limiting the plasma performance achievable.

It is expected that fusion-born α particles will result in very long sawtooth periods in ITER [38–40]. Indeed, alpha-tail production with ICRF heating of He^4-beam ions in JET confirmed that the energetic α particles result in "monster" sawteeth [41, 42], which are loosely defined as sawteeth with periods longer than the energy confinement time, and hence saturated central plasma temperature. The resultant long period sawteeth are more likely to trigger NTMs, and therefore the control of sawteeth is vital. The two approaches to sawtooth control are to attempt to suppress sawteeth for many energy confinement times (i.e. *stabilise* the kink mode) or to deliberately decrease the sawtooth period (i.e. *destabilise* the kink mode). The baseline scenario in ITER is predicated upon using the sawteeth to reverse the on-axis accumulation of higher-Z impurities that would otherwise cause degradation of energy confinement due to impurity radiation. The approach currently adopted for sawtooth control in baseline scenarios in ITER is to deliberately destabilise the internal kink mode to give frequent, small amplitude sawtooth crashes. A lower limit in the sawtooth period is determined by the slowing down time of the fusion α particles, since the energetic α particles must transfer their energy to the thermal plasma core to ensure continuing fusion reactions.

In Sect. 4.2, recent developments in the theoretical understanding of sawtooth stability are discussed. Models that predict the conditions under which a sawtooth crash will occur are also outlined. Sawtooth control achieved by locally perturbing the current profile is discussed in Sect. 4.3. Recent results exhibiting destabilisation of sawteeth by steerable electron cyclotron resonance heating (ECRH) are presented, including real-time feedback schemes and electron cyclotron current drive (ECCD) control in the presence of energetic ions in the plasma core. These results justified the inclusion of ECCD for sawtooth control in the ITER design [10].

Sawtooth control can also be achieved by changing the gradients of the fast particle distribution. In Sect. 4.4, sawtooth behaviour in plasmas heated by neutral beam injection (NBI) is examined. Understanding how the fast ions affect the sawteeth in these NBI experiments has implications for how sawtooth control can be achieved with ion cyclotron resonance heating (ICRH). ICRH has been used to destabilise sawteeth, as described in Sect. 4.5 through both current drive and kinetic effects. Finally, the application of these sawtooth control techniques in ITER is discussed in Sect. 4.6.

4.2 The Physics of Sawtooth Stability

Since a sawtooth crash is usually accompanied by an $m = n = 1$ kink displacement [43], it is important to understand the factors which influence the stability of the 1/1 internal kink mode. In regions of high current there is a strong poloidal magnetic

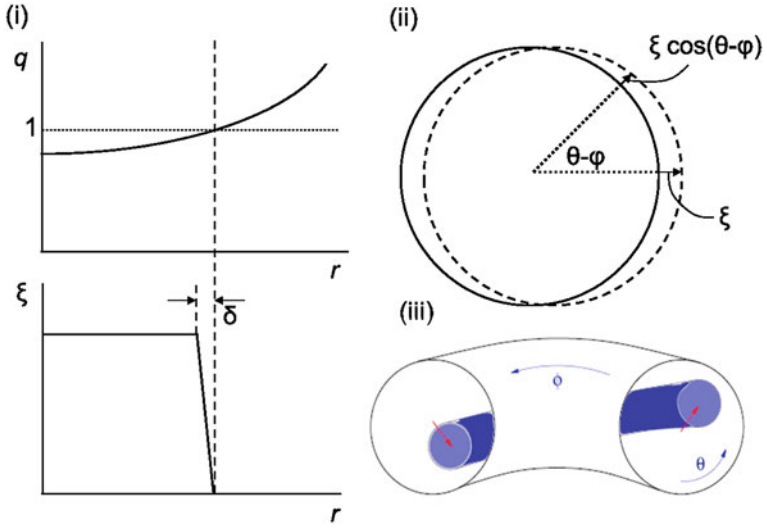

Fig. 4.4 (i) The radial dependence of the $n = m = 1$ internal kink mode, localised at the $q = 1$ surface (ii) the displacement of a circular flux surface for an $m = 1$ perturbation and (iii) the distortion of an $n = m = 1$ kink in a toroidal geometry

field induced by the current. Should the plasma then experience a perturbation, the strong poloidal magnetic field will reinforce the instability and push the plasma further out, extending the "kinking" effect [2]. The $n = m = 1$ internal kink mode takes the radial structure of a top-hat displacement which is rigid within the $q = 1$ surface and zero outside, as depicted in Fig. 4.4 However, sawtooth stability in tokamak plasmas is not determined solely by the fluid drive of the 1/1 internal kink mode; its dynamics are significantly affected by the presence of energetic particles, by sheared flows, by diamagnetic effects, by pressure anisotropy, by complex nonlinear reconnection physics and local effects in the inertial layer around the $q = 1$ surface. All of these effects have implications for the actuators which can be utilised to control sawteeth, as discussed below.

4.2.1 Effect of Energetic Particles

High power ion cyclotron resonance heating (ICRH) experiments in JET showed that the sawtooth instability could be suppressed for many seconds [44] and that long sawtooth quiescent periods were terminated abruptly by a sawtooth collapse that followed the switch off of the ICRH [45]. The inference from this was that the fast ions induced by ICRH provided a stabilising influence upon the 1/1 kink mode, and thus the sawteeth. This was later confirmed using fast ions from NBI [13] and fusion-born α particles [46].

There followed a significant theoretical effort to explain this phenomenon, largely building on the principles developed by Chen et al. [47] to explain the fishbone instability [48]—another $m = n = 1$ internal kink instability driven by gradients in the fast particle pressure. The dispersion relation [49–51] gives

$$i\sqrt{\omega(\omega - \omega_{*i})} \sim \delta W_{MHD} + \delta W_{hf} + \delta W_{hk} \tag{4.1}$$

where δW_{hf} and δW_{hk} are the fluid and kinetic components of the change in the potential energy of the kink mode due to the energetic particles respectively. This equation and $\delta \hat{W}_{MHD}$ is the ideal fluid mode drive [52, 53] was found to have two branches: The first, when $\Re e(\omega) \sim \langle \omega_{dh} \rangle$ and $\langle \omega_{dh} \rangle$ is the bounce-averaged magnetic drift frequency of the hot ions, characterises the fishbone instability [47]. The second, when $\Re e(\omega) < \langle \omega_{dh} \rangle$, relates to the sawteeth. The trapped energetic ions give rise to significant stabilisation providing the lower frequency branch satisfied the condition:

$$\Re e(\omega) \ll \langle \omega_{dh} \rangle \tag{4.2}$$

Kruskal and Oberman [54] also showed that thermal ions can stabilise core MHD instabilities. This was later confirmed using the energy principle including the guiding centre motion of the energetic particles [55–57]. In the next sections we consider the contributions of various energetic particles to the change in the potential energy of the mode (as in 4.1), beginning with bounce-trapped particles.

4.2.1.1 Trapped Energetic Ions

The stabilisation of low-frequency MHD perturbations by trapped fast ions is a consequence of the conservation of the third adiabatic invariant [58, 59]. Porcelli proposed that in a tokamak this third adiabatic invariant of motion [60], Φ_{ad}, is equivalent to the flux of the poloidal magnetic field through the area defined by the toroidal precession of the trapped particle orbit centres. The fast ions can be viewed as a distribution of current loops (in equilibrium with the fast particle pressure) [58]. The current in each of these loops is analogous to the precessional drift frequency of the trapped particle. These loops have a poloidal flux through the area which they enclose. If the plasma experiences an $n/m = 1/1$ displacement, the poloidal flux through this area would change. For instance, the kink depicted in Fig. 4.5 causes the poloidal flux through the area defined by the banana orbit centres to increase. However, the fast ions respond in order to conserve Φ_{ad}, and in so-doing, the loops can contract or expand, or shift and tilt in space. For the case shown in Fig. 4.5, and with the fast ion pressure peaked on-axis, the current loops will contract, which requires an increase in the energy of the fast ions. This energy is taken from the mode, and so the presence of the fast ions results in a stabilisation of the sawteeth.

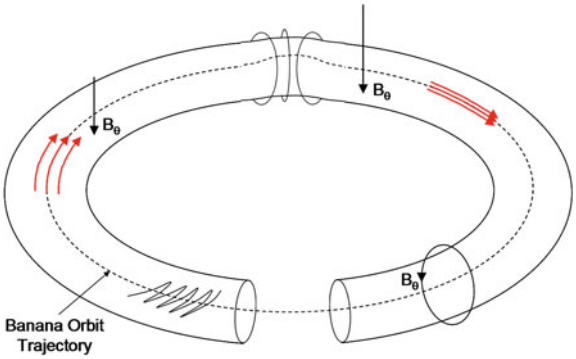

Fig. 4.5 The fast particles can be considered as current loops, whose amplitude is proportional to their precessional drift frequency. The poloidal flux through the area defined by the toroidal revolution of the banana centres is conserved. This figure shows a schematic time evolution depicting a kink displacements, which causes the loops to contract in order to conserve the poloidal flux, taking energy from the mode and so stabilising the sawteeth

By employing the generalised energy principle, the change in the potential energy of the kink mode due to the energetic trapped ions can be calculated, giving [58, 61, 62]

$$\delta W_h = \frac{1}{2}\int \mathrm{d}\Gamma (M v_\parallel^2 + \mu B)\delta f_h \sum_m \boldsymbol{\kappa}\cdot\boldsymbol{\xi}^{(m)*}(r,t)e^{-i(n\phi - m\theta)} \tag{4.3}$$

where θ is the poloidal angle, $\boldsymbol{\kappa} = \mathbf{b}\cdot\nabla\mathbf{b}$ is the magnetic curvature vector and $\mathbf{b} = \mathbf{B}/B$. This then needs the calculation of the change in the fast particle distribution function, δf_h to be assessed. The fast ion distribution function is typically separated into an equilibrium component, $f_0(\mathcal{E}^0, \mathcal{P}_\phi^0, \mu)$, and two perturbed components, $\delta f_h = \delta f_{hk} + \delta f_{hf}$, a non-adiabatic (kinetic) and an adiabatic (fluid) part respectively. Here, an adiabatic particle has characteristic motion around a closed orbit much faster than the temporal and spatial scales associated with the perturbation (i.e. the perturbation appears as a static modification of the equilibrium). The particle energy ($\mathcal{E}^0 = Mv^2/2$), the canonical momentum ($\mathcal{P}_\phi^0 = MB_\phi v_\parallel/B - e\psi_p$) and the magnetic moment ($\mu = Mv_\perp^2/2B$) are the unperturbed constants of motion, where M is the particle mass, e is the charge and ψ_p is the poloidal flux at the particle position. Analytic theory developed for large aspect ratio circular plasmas [61] can be used to express these contributions to the perturbed distribution function as

$$\begin{aligned}\delta f_{hk} = \sum_{l=-\infty}^{\infty} &\frac{\tilde{\omega} - \Delta\Omega - n\omega_{*h}}{\tilde{\omega} - \Delta\Omega - n\langle\omega_{dh}\rangle + l\omega_b}\frac{\partial f_h}{\partial \mathcal{E}^0} e^{-i(\omega + l\omega_b + n\langle\omega_{dh}\rangle)t} \\ &\times \left\langle (v_\parallel^2 + \frac{v_\perp^2}{2})\kappa\cdot\xi_\perp e^{i(\omega + l\omega_b + n\langle\omega_{dh}\rangle)}\right\rangle\end{aligned} \tag{4.4}$$

$$\delta f_{hf} = -\frac{Ze}{M_h}\,\xi\cdot\nabla\psi_p\frac{\partial f_h}{\partial \mathcal{P}_\phi^0} \tag{4.5}$$

respectively, where $\omega_{*h} = (\partial f_h/\partial\mathcal{P}_\phi^0)/(\partial f_h/\partial\mathcal{E}^0)$ is the hot ion diamagnetic frequency, $\omega_b = 2\pi/\tau_b$, τ_b is the poloidal orbit transit time, M_h is the fast ion mass, the dots represent the derivative with respect to time, $\Delta\Omega = \Omega_E(r) - \Omega_E(r_1)$ is the sheared toroidal flow, $\tilde{\omega}$ is the Doppler shifted mode frequency, l is the poloidal quantum number and $\langle\cdots\rangle$ defines an average. The important thing to notice from 4.4 is that a large stabilising contribution can occur when the Doppler-shifted mode frequency is balanced by the characteristic orbit frequencies of the particles, at which point the denominator becomes very small. When this resonance condition is satisifed, the trapped energetic particles have a strong influence on the dynamics of the sawteeth.

Finally, it is worth noting that NBI did not stabilise sawteeth as effectively as ICRH [64]. This is partially because NBI minority ions are far less energetic than ICRH ions, meaning that they were less likely to satisfy the condition for conservation of Φ_{ad}: $\Re e(\omega) \ll \langle\omega_{dh}\rangle$, but also due to greater plasma rotation, flow shear and anisotropy achieved with NBI [63, 65, 66]. NBI also gives rise to a much larger fraction of passing ions, whose effect is discussed below.

4.2.1.2 Passing Energetic Ions

For very energetic ions, the radial drift motion becomes comparable to the radial extent of the kink mode. In this regime, the kinetic contribution to the mode's potential energy associated with the passing fast ions becomes increasingly important when the passing fast ion population is asymmetric in velocity space [67–69]. The contribution from the circulating particles arises primarily from the ions close to the trapped-passing boundary where their orbit widths, Δ_b are large, $\delta W_h^p \sim \Delta_b$. The effect of passing ions is enhanced for large effective orbit widths [70], which is to say, for highly energetic ions (like ICRH or N-NBI in ITER) or for a population with a large fraction of barely passing ions (like NBI in JET). Passing fast ions can destabilise the internal kink mode when they are co-passing and the fast ion distribution has a positive gradient across $q = 1$, or when they are counter-passing, but the deposition is peaked outside the $q = 1$ surface. First let us consider the case of on-axis co-NBI. When a co-passing beam ion is born inside the $q = 1$ surface it experiences an inward ∇B drift, which means that it stays within the $q = 1$ surface and never crosses it. The distribution function has a negative hot particle pressure gradient, $\nabla\langle P_h\rangle < 0$, so this particle will give a stabilising contribution when in the region of good curvature, but will be destabilising when in the region of adverse curvature on the outboard side. These two contributions tend to cancel, and the beam ions inside $q = 1$ (which make up the majority of on-axis NBI ions) do not affect the mode stability. However, the few ions which are born outside $q = 1$ will only pass through the $q = 1$ surface in the

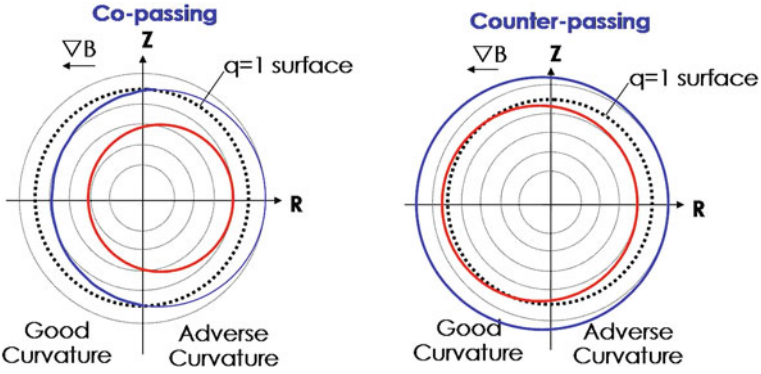

Fig. 4.6 The co-passing ions experience a downwards ∇B-drift, which causes ions born inside the $q = 1$ surface to stay inside $q = 1$, and those born outside it, to only cross the $q = 1$ surface in the region of good curvature. This means that distributions with a fast ion pressure peaked inside $q = 1$ are stabilising, whereas those with a pressure peaked outside $q = 1$ are destabilising. The opposite is true of counter-passing ions

region of good curvature due to the inward ∇B drift. As such, these will give a stabilising contribution to the kink mode (since for $q > 1$, $\xi = 0$). Intuitively the opposite is true for counter-passing ions which have an opposite ∇B drift upward from their flux surface; those ions born inside $q = 1$ will only contribute in the region of adverse curvature. Since they have a negative hot particle pressure gradient, the contribution from counter-passing ions is destabilising. Consequently, the $n/m = 1/1$ internal kink mode is stabilised by co-passing on-axis NBI ions or by counter-passing off-axis NBI ions, but is destabilised by counter-passing on-axis NBI ions or co-passing off-axis NBI ions. This effect is illustrated in Fig. 4.6. This mechanism depends strongly on the local gradient $\partial f_h/\partial P_\zeta$ at the $q = 1$ surface and as such is sensitive to localised heating. This mechanism is described in detail in [68] and [71] with an overview of fast ion effects in [70].

4.2.2 Effect of Toroidal Rotation

4.2.2.1 Equilibrium Mass Flow of the Order of the Sound Speed

As well as giving rise to a population of energetic particles, NBI also results in a toroidal rotation of the plasma, sometimes approaching the ion sound speed [72]. At rotation which is a significant fraction of the sound speed, the centrifugal effects can also affect kink mode stability, [73, 74]. Subsequent modelling of the effects of sheared toroidal flows on MHD modes found that rotation approaching the ion sound speed could completely stabilise the ideal $n = 1$ kink mode [75, 76], implying that the longer quiescent periods observed in NBI heated plasmas were

not only due to the fast ions, but also the ancillary stabilising effect arising from the beam-driven plasma rotation. It is worth noting that calculations of the stability of the internal kink mode are highly sensitive to including rotation in the formulation of the initial equilibrium [77] as well as the precise density and rotation profiles [78].

4.2.2.2 Flows of the Order of the Diamagnetic Velocity

Even at slow rotation speeds of the order of ω_{*i}, the *shear* of the rotation profile can affect the stabilisation arising from the trapped ions. Conservation of the third adiabatic invariant, Φ_{ad} is only obtained [65] when $\langle\omega_{dh}\rangle + \Delta\Omega - \tilde{\omega} \gg 0$. This can be seen from the denominator in 4.4. Since this condition is more readily satisfied for co-rotation ($\Delta\Omega > 0$), plasmas with co-I_P velocity shear support more effective stabilisation of the kink mode, whereas the stabilising effect is diminished in counter-rotating plasmas ($\Delta\Omega < 0$). The plasma flow will only influence mode stability when $|\Delta\Omega| \sim \omega_{*i}$, which is unlikely to be met in ITER.

4.2.3 Sawtooth Crash Trigger Modelling

The fundamental trigger of the sawtooth crash is the onset of an $m = n = 1$ mode. The dynamics of this instability are constrained by many factors including not only the macroscopic drive from ideal MHD, but collisionless kinetic effects related to high energy particles described in Sect. 4.2.1 and rotation effects described in Sect. 4.2.2, as well as non-ideal effects localised in the narrow layer around $q = 1$. The phenomenology of sawtooth oscillations and their theoretical interpretation is reviewed in [1, 79–81].

Advances in the experimental diagnosis of the sawtooth cycle have led to the proposal of many crash trigger models, including full reconnection [82], resistive two-fluid MHD [83, 84], collisionless kinetic effects [54, 55, 85], accelerated complete reconnection due to nonlinear collisionless effects [86], magnetic stochastisation which led to enhanced perpendicular transport [87], chaos [88], the quasi-interchange model [89], the localised reconnection model [90, 91] and triggering of secondary instabilities [92–96]. In the partial reconnection model, the magnetic surfaces begin to undergo reconnection, just as in the full reconnection Kadomtsev model [82]. However, when the magnetic island reaches a critical width, the core region and critical island region undergo different relaxation processes. The inner core Taylor relaxes, as proposed in [92], whilst the reconstructed surfaces in the island region have the same helical flux, as in full reconnection. This partial reconnection [97] results in the formation of two current sheets, which diffuse rapidly during the ramp phase of the subsequent sawtooth.

A heuristic model developed using linear theory suggests that a sawtooth crash will occur when one of the following criteria is met [38, 96]:

$$-\delta\hat{W}_{core} > c_h\omega_{dh}\tau_A \tag{4.6}$$

$$-\delta\hat{W} > \frac{1}{2}\omega_{*i}\tau_A \tag{4.7}$$

$$-c_\rho\hat{\rho} < -\delta\hat{W} < \frac{1}{2}\omega_{*i}\tau_A \quad \text{and} \quad \gamma_{eff} > \frac{1}{c_*}\sqrt{\omega_{*i}\omega_{*e}} \tag{4.8}$$

where ω_{dh} is the magnetic drift frequency of the hot ions, $\tau_A = \sqrt{3R}/v_A$ is the Alfvén time, c_h, c_ρ and c_* are normalisation coefficients of the order of unity, γ_{eff} is the effective growth rate of the resistive internal kink mode [98] and $\hat{\rho} = \rho_i/r_1$. The change in the kink mode potential energy is defined such that $\delta\hat{W}_{core} = \delta\hat{W}_{MHD} + \delta\hat{W}_{KO}$ and $\delta\hat{W} = \delta\hat{W}_{core} + \delta\hat{W}_h$ where $\delta\hat{W}_{KO}$ is the change in the mode energy due to the collisionless thermal ions [54], $\delta\hat{W}_h$ is the change in energy due to the fast ions. The potential energy is normalised such that $\delta\hat{W} \equiv 4\delta W/(s_1\xi_0^2\varepsilon_1^2RB^2)$ The second part of (4.8) can be recast in terms of a critical magnetic shear determined by the pressure gradient, $s_1 > s_{crit}(\omega_{*i})$,

$$s_1 > \max(s_{crit} = \frac{4\delta W}{\xi_0^2\varepsilon_1^2RB^2c_\rho\hat{\rho}}, s_{crit}(\omega_*)) \tag{4.9}$$

The linear stability thresholds presented in 4.6–4.9 are useful for understanding when an $n = 1$ internal kink mode will stimulate a sawtooth crash, whilst the nonlinear dynamics of the crash phase and how the profiles are affected are not considered. It is evident from 4.9 that sawteeth can be stimulated by enhancing s_1 (through localised current drive), or reducing δW. Despite its heuristic formulation based solely on linear stability thresholds, the model proposed by Porcelli et al. [38] has had notable success when compared to the observed sawtooth phenomenology in tokamak plasmas [97, 99–101].

4.2.4 Sawtooth Control Actuators

Sawtooth control refers to the ability of an actuator (be it a heating and/or current drive system or plasma shaping control) to alter the likelihood of triggering other MHD instabilities, usually quantified by the sawtooth period. This can be achieved by tailoring the distribution of energetic ions; by changing the radial profiles of the plasma current density and pressure, notably their local gradients near the $q = 1$ surface; by rotating the plasma, or changing the rotation shear local to the $q = 1$ surface; or by heating the electrons inside the $q = 1$ surface. The primary actuators

to achieve these perturbations are electron cyclotron current drive (ECCD) (Sect. 4.3), neutral beam injection (NBI) (Sect. 4.4) and ion cyclotron resonance heating (ICRH) (Sect. 4.5).

By driving current just inside the $q = 1$ surface, the magnetic shear at $q = 1$ can be increased, resulting in more frequent sawtooth crashes. This can be understood by considering 4.9 where the linear crash criterion is satisfied when the magnetic shear at $q = 1$ is sufficiently large. Data from TFTR plasmas [102] showed that sawteeth occurred when the magnetic shear at $q = 1$ exceeded a critical value given by collisionless theory [103] strongly supporting the enhancement of the magnetic shear as a sawtooth control actuator. ECCD is the primary sawtooth control actuator in the ITER design [10] due to both the highly localised current density that can be achieved and the ability to provide real time control by changing the launcher angle of the injected EC beam with steerable mirrors. However, some concerns remain regarding the ability of ECCD to destabilise sawteeth in the presence of a significant population of energetic particles inside $q = 1$, as in ITER. This concern is exemplified by 4.8 where the left hand side, ρ/r_1, will be very small since ρ is small and r_1 is predicted to extend towards mid-radius in ITER baseline scenario, whilst the right hand side is likely to have a large δW_h in the numerator due to the presence of the α particles. Fortunately, NBI and ICRH can influence the magnitude of δW directly.

Neutral beam injection affects the change in the potential energy of the internal kink mode in two ways: Firstly, it gives rise to a significant population of energetic particles in the plasma. The predominantly passing fast ions can destabilise the sawteeth when they are injected in the same direction as the plasma current and outside the $q = 1$ surface, or opposite to the plasma current and inside $q = 1$. Secondly, NBI also results in a torque on the plasma, and significant toroidal rotation can stabilise the internal kink mode too. However, due to the rather broad $q = 1$ surface expected in ITER [10], the N-NBI energetic ions are likely to be born inside $q = 1$, even when injected at the most tangential angle of injection [40], meaning that (at least for co-NBI) they will always be strongly stabilising and cannot be used to shorten the sawtooth period.

Conversely, ion cyclotron resonance heating can give rise to a population of energetic particles outside $q = 1$ in ITER. Initial studies of the effects of ICRH on sawtooth behaviour concluded that the (de)stabilisation achieved arose due to the driven current changing the magnetic shear local to $q = 1$. However, recent studies have shown that ICRH sawtooth control persists in plasmas where the driven current is negligible, highlighting that the ICRH destabilisation mechanism also includes strong kinetic effects. For instance, it has been shown [71, 104] that the fast ion population born due to off-axis ^{3}He minority RF-heating scenarios, like the operating scenario proposed for ITER, can give rise to sawtooth destabilisation, even in the presence of core fast ions.

4.3 Current Drive Schemes

When electron cyclotron resonance heating (ECRH) is applied to the plasma, a change in the local current density occurs due to the change in the temperature, and subsequent change in the conductivity. This in turn modified the magnetic shear at $q = 1$, s_1, affecting the likelihood of a sawtooth crash, as seen in 4.9. By adding a toroidal component to the wave vector of the launched EC waves, an ancillary electron cyclotron driven current results either parallel (co-ECCD) or anti-parallel (counter-ECCD) to the Ohmic current, enhancing the potential to alter s_1.

Early experiments to assess the applicability of sawtooth control using current drive schemes focussed on sawtooth stabilisation [9, 105–108]. It was demonstrated that careful placement of the ECCD deposition location could stabilise the sawteeth for the entire gyrotron pulse length on WT-3 (0.03 s) [109], TEXTOR (0.2 s) [110], JT-60U (1.5 s) [111] and ASDEX Upgrade (2.0 s) [112]. Soon after, sawtooth destabilisation was also achieved [113]. ECCD is more effective than ECH (here defined as when the beam injection angle is perpendicular to the magnetic axis) [114, 115], although electron heating does have an indirect effect on the current by changing the local resistivity profile. Furthermore, the effect on the sawteeth can be enhanced by maximising the local ECCD current density rather than the total driven current by narrowing the deposition width [116]. In all cases, significant changes in the sawtooth period occur for very small changes in the deposition location (of the order of the deposition width, typically a few cm) with respect to the location of the $q = 1$ surface [106]. It is this strong localisation of the driven current which makes ECCD a robust sawtooth control actuator, even when the driven current is as little as 1 % of the Ohmic current [117–119]. Sawtooth control using ECCD has been demonstrated in a number of devices including T-10 [120], ASDEX Upgrade [114, 116, 121, 122], TCV [100, 117, 123, 124], JT-60U [111, 125], DIII-D [115], TEXTOR [20, 110], Tore Supra [126–128], FTU [129] and WT-3 [130].

By sweeping the EC deposition location across the $q = 1$ surface (by ramping the magnetic field) it was found that the sawtooth period was highly sensitive to the location of the deposition with respect to the sawtooth inversion radius [107, 108, 131]. Increasing the current inside $q = 1$ increases s_1 and so destabilises the sawteeth, whilst co-ECCD localised just outside $q = 1$ decreases s_1 and so stabilises the sawteeth. Conversely, counter-ECCD just inside $q = 1$ results in stabilisation and just outside $q = 1$ gives rise to destabilisation [100, 114, 118, 119]. This behaviour is demonstrated in Fig. 4.7, showing the sawtooth period with respect to the deposition location of the ECCD in TEXTOR [110], as well as in many other machines [100, 107, 108, 114, 131]. ECCD power scans have also shown that as the driven current is increased, the effect on the sawtooth behaviour is enhanced [114, 132]. Finally, it is worth noting that the control of sawteeth for NTM prevention using ECCD has been demonstrated directly on ASDEX Upgrade. Reference [121] shows that NTMs are avoided at high β_N by complete suppression of the sawteeth using co-ECCD just outside the $q = 1$ surface. Concomitant with the end of the

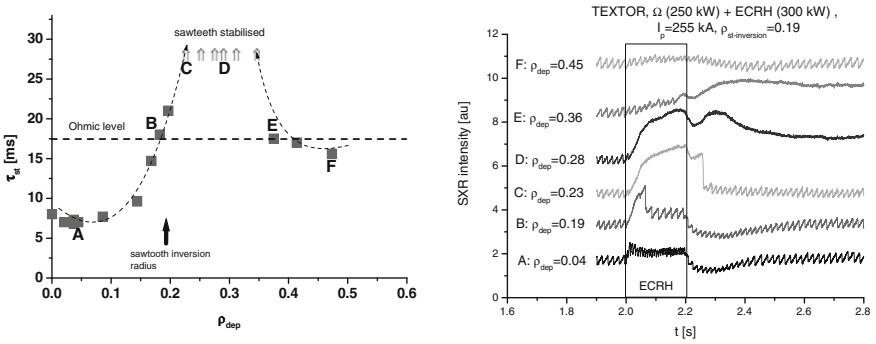

Fig. 4.7 (*left*) The sawtooth period as a function of ECRH deposition location in TEXTOR compared to the inversion radius. The letters refer to discharges shown in the (*right*) figure. Reproduced with permission from "Electron cyclotron resonance heating on TEXTOR" [110]

gyrotron pulse, a sawtooth crash occurred and an NTM was triggered, resulting in a substantial degradation of the plasma performance.

In parallel to the extensive experimental evidence of sawtooth control via current drive, complementary numerical modelling improved the understanding of the physical mechanisms underlying this actuator. Discharges with ECH, and co- and counter-ECCD in TCV have been modelled using the PRETOR-ST code [100, 117]—a transport code including a model for determining when a sawtooth crash will occur based on the linear stability thresholds given in [38]. The modelling shows that whilst co- and counter-current drive have opposite effects, the anti-symmetry is broken by ancillary localised heating. Since the heating acts like co-ECCD, the most efficient destabilisation occurs with co-ECCD and ECH just inside the $q = 1$ surface, whilst the most efficient stabilisation occurs with co-ECCD and ECH outside $q = 1$ [100]. Figure 4.8 shows the sawtooth period in TCV compared to numerical prediction from transport modelling when one ECH beam is oriented just outside $q = 1$ to stabilise the sawteeth and a second beam swept outwards across the inversion radius. The simulations accurately predict the sawtooth period and behaviour during the ECCD sweep, despite using a full reconnection model. Similar ASTRA [133] modelling was used to explain the difference between co- and counter-ECCD on ASDEX Upgrade, once again identifying the change in the magnetic shear as the reason for the change in sawtooth behaviour [114].

However, whilst the experiments using magnetic field ramps to alter the deposition location of the ECCD have significantly improved the understanding of the control mechanisms, a major advantage of current drive schemes is that the angle of inclination of the EC launcher mirrors provides a simple external actuator in a feedback-control loop. Indeed, the uncertainties in the control parameters (such as the launcher aiming and ray-tracing prediction for the resultant driven current) and the plasma equilibrium parameters (such as the $q = 1$ location and plasma position), coupled with the strong sensitivity of the sawtooth period to the deposition location relative to $q = 1$, mean that real-time feedback is a necessity for robust control reliant upon current drive schemes. TCV has demonstrated

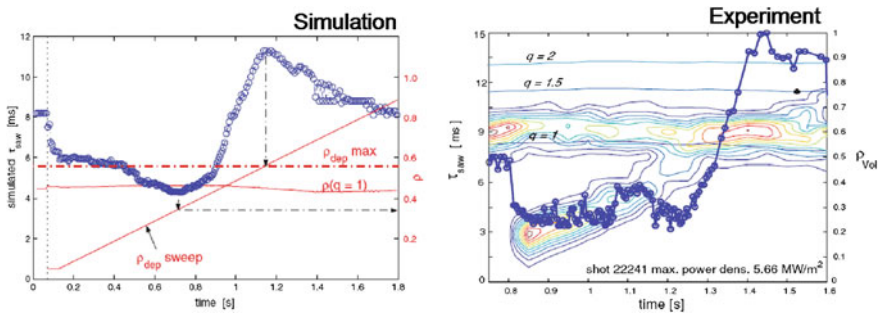

Fig. 4.8 (*left*) Predictions of the sawtooth period from the PRETOR-ST code and (*right*) the measured sawtooth period in TCV with ECH beams directed on-axis to stabilise the sawteeth and an ancillary ECH beam is swept across the inversion radius. The contours in the *right figure* indicate the location of the heat deposition relative to the minor radius, r. Reproduced with permission from "Effects of localized electron heating and current drive on the sawtooth period" [100]

sawtooth control in real-time feedback by varying the EC launcher injection angle in order to obtain a pre-determined sawtooth period [134, 135] or to maximise the sawtooth period [136]. Figure 4.9 shows that by changing the launcher angle, and therefore modifying the magnetic shear around $q = 1$, the observed sawtooth period in TCV can be forced to track a requested period. The time lag between the change in the requested period and that achieved is determined by the nonlinear

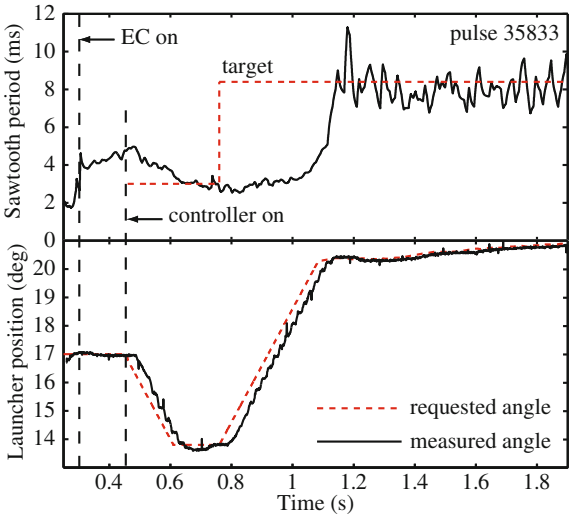

Fig. 4.9 The sawtooth period observed in TCV when real-time ECCD control is applied. The control algorithm successfully achieves and tracks two levels of requested sawtooth period by moving the ECH launcher angle to change the deposition location, and consequently the magnetic shear at $q = 1$ accordingly. Paley et al. [135] published by Institute of Physics Publishing. © IOP Publishing. Reproduced with permission. All rights reserved

plasma response and movement of the $q = 1$ radius. Tore Supra have implemented a 'search and maintain' control algorithm to vary the ECCD absorption location in search of a location at which the sawtooth period is minimised; having achieved this, the controller maintains the distance between the ECCD deposition location and the measured inversion radius despite perturbations to the plasma [128]. Recently, fine control over the sawtooth period has been demonstrated on TCV using either 'sawtooth pacing' via modulated ECCD with real-time crash detection [137], or 'sawtooth locking', where the sawtooth period is controlled even in the absence of crash detection in a reduced region of duty-cycle v pulse-period parameter space [138, 139].

The residual concern for sawtooth control with current drive in ITER is whether changes in s_1 can overcome the stabilisation arising in the presence of energetic particles, as described in Sect. 4.2.1. The change in the magnetic shear may need to be substantial to compete with the kinetic stabilisation of the kink mode, especially if the fast ions arising from concurrent ICRH and NBI heating exacerbate the inevitable effect of the alpha particles. Consequently, recent experiments have attempted to demonstrate destabilisation of sawteeth via driven current despite the presence of energetic particles. Sawtooth destabilisation of long period sawteeth induced by ICRH generated core fast ions with energies ≥ 0.5 MeV has been achieved in Tore Supra, even with modest levels of ECCD power [127]. Figure 4.10

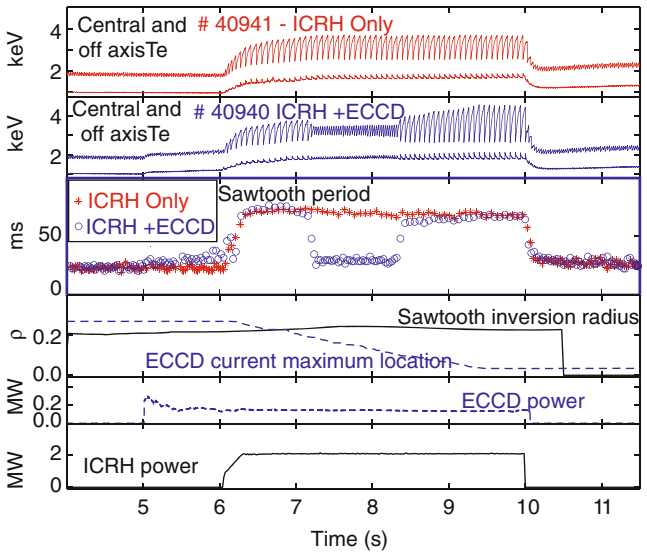

Fig. 4.10 Demonstration of sawtooth destabilisation in the presence of core fast ions in Tore Supra. Two consecutive shots with 2.3 MW of ICRH with and without co-ECCD are shown. The radial ECCD deposition location was scanned from outside the sawtooth inversion radius to the plasma centre. When the deposition was just inside $q = 1$ the sawtooth period dropped to approximately the level of Ohmically heated plasmas, despite the stabilising ICRH ions in the plasma core. Reprinted figure with permission from Lennholm et al. [127]. Copyright 2009 by the American Physical Society

shows the sawtooth period in Tore Supra discharges, with just ICRH heating in the plasma core and with ancillary ECCD swept across the $q = 1$ surface respectively. The ICRH fast ions lead to long sawtooth periods, but the ECCD is able to drop the sawtooth period back to the level of Ohmically heated plasmas when the deposition is optimally located just inside the $q = 1$ surface despite the presence of highly energetic ions. Similar ECCD destabilisation has also been achieved in the presence of ICRH accelerated NBI ions in ASDEX Upgrade [140] as well as with normal NBI fast ions in ASDEX Upgrade [114], JT-60U [125] and HL-2A [141].

More recently sawtooth control using ECCD has even been demonstrated in ITER-like plasmas with a large fast ion fraction, wide $q = 1$ radius and long uncontrolled sawtooth periods in DIII-D [142]. Active sawtooth control using driven current inside $q = 1$ allows the avoidance of sawtooth-triggered NTMs, even at much higher pressure than required in the ITER baseline scenario. Operation at $\beta_N = 3$ without 3/2 or 2/1 neoclassical tearing modes has been achieved in ITER demonstration plasmas when sawtooth control is applied using only modest ECCD power [142]. Such avoidance of NTMs permitting operation at higher pressure than otherwise achievable by application of core ECCD sawtooth control has also been demonstrated in ASDEX Upgrade [143]. Figure 4.11 demonstrates how modest ECCD directed inside the $q = 1$ surface has been utilised in DIII-D to keep the sawtooth period short, thereby avoiding triggering of NTMs,

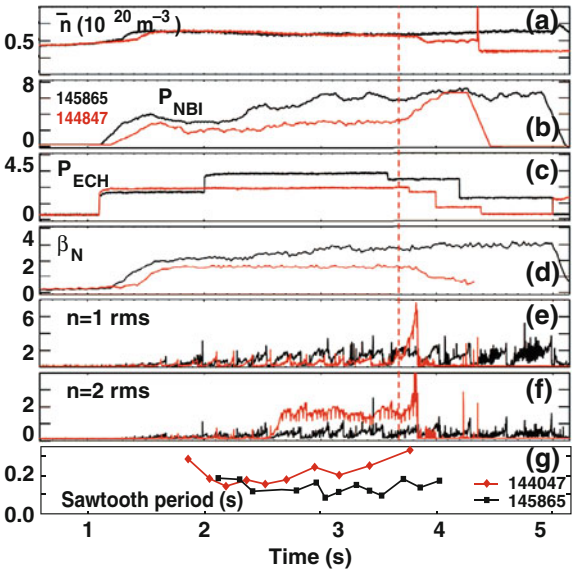

Fig. 4.11 The electron line density, NBI power, ECH power, normalised beta and the rms amplitude of the $n = 1$ and $n = 2$ instabilities in DIII-D discharges 144847 (*red*, no active sawtooth control) and 145865 (*black*, with active sawtooth control). Whilst a 2/1 NTM is triggered at 3.7 s after a sawtooth crash in 144847, when $\beta_N = 1.8$, much higher performance is achieved for much longer with active sawtooth control, allowing $\beta_N \approx 3$. Reproduced with permission from "Sawtooth control using electron cyclotron current drive in ITER demonstration plasmas in DIII-D" [142]

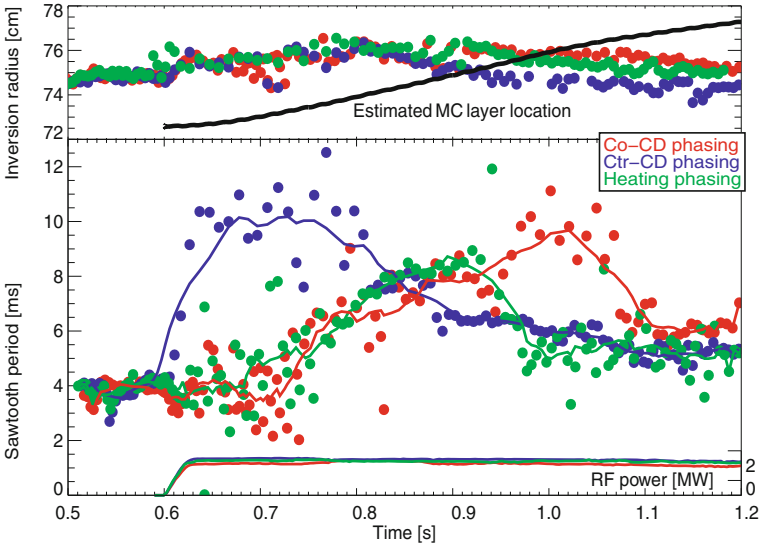

Fig. 4.12 Sawtooth control via changing the magnetic shear by mode conversion current drive demonstrated on Alcator C-Mod. As the mode conversion layer is moved from inside to outside the inversion radius, the sawtooth period is found to increase then decrease for counter-current drive phasing. For both co-propagating ICRH waves and pure heating phasing the sawtooth period decreases then increases. The symmetric phasing results in a co-current due to the strong up-down asymmetry. Reprinted figure with permission from Parisot et al. [148] published by Institute of Physics Publishing.

and consequently achieving higher plasma pressure than would otherwise be possible. This is done in the presence of high core fast ion fractions with strong auxilliary heating, akin to the situation expected in ITER.

Finally, it should be noted that other current drive actuators can also affect sawtooth behaviour. For instance, Lower Hybrid Current Drive (LHCD) has been used to control sawteeth [144–146], as has Mode Conversion Current Drive (MCCD) [147, 148]. Figure 4.12 shows the sawtooth period as a function of the radial location of the mode conversion layer in Alcator C-Mod plasmas as the toroidal field is varied to move the resonance from inside to outside the inversion radius. Just as in the ECCD experiments, the change in the local magnetic shear due to co-(counter-) current MCCD causes the sawtooth period to in(de)crease then de(in)crease respectively as the MCCD deposition is swept from inside to outside $q = 1$.

4.4 Neutral Beam Injection

Neutral beam injection affects sawtooth behaviour through both the introduction of energetic particles as well as the torque applied to the plasma. Having said that, NBI is not considered as a sawtooth control actuator for ITER because the broad

$q = 1$ radius expected in the ITER baseline operating scenario means that the NBI-induced energetic ions will always be inside $q = 1$, and thus strongly stabilising. Nonetheless, NBI-heated plasmas are useful for understanding the physical mechanisms that affect mode stability, as well as providing a tool for sawtooth control in present-day devices.

It has been known for some time that NBI heating could strongly stabilise the kink mode and lead to long sawtooth periods [13], an effect attributed to the stabilisation arising in the presence of a population of core energetic trapped ions, as described in Sect. 4.2.1, as well as stabilisation occurring in strongly rotating plasmas, as outlined in Sect. 4.2.2. Later, it was observed that strong sawtooth stabilisation occurred when heated with 350 keV Negative-ion neutral beam injectors (N-NBI) [149], despite the resulting fast ion population being predominantly passing, giving rise to studies of the influence of circulating ions on the stability of the $n = 1$ internal kink mode. As described in Sect. 4.2.1, destabilisation of the internal kink mode can occur when $\partial f_h(v_\parallel > 0)/\partial r > \partial f_h(v_\parallel < 0)/\partial r$, which occurs when the energetic ions are injected either off-axis ($\partial f_h/\partial r > 0$) and oriented with the plasma current, or when the fast ion population is predominantly on-axis ($\partial f_h/\partial r > 0$) and directed opposite to the plasma current. This effect has been demonstrated by experiments that exhibit an asymmetry in sawtooth behaviour depending upon whether the NBI is injected co-I_p, or counter-current [76, 150, 151]. The asymmetry observed in JET [150] was explained by the competition between the stabilising trapped ions and the destabilising counter-passing ions in the counter-NBI regime, compared with two complementary stabilising effects for co-NBI. Whilst the amplitude of the rotation is strongly sub-Alfvénic, such that gyroscopic effects as outlined in Sect. 4.2.2 play a small role, the flow *shear* at $q = 1$ can be significant, and reduces the stabilising effect of the trapped ions when $\Delta\Omega < 0$, as explained in Sect. 4.2.1. The fact that the finite orbit width of these relatively low energy NBI passing ions could play such an important role in determining sawtooth stability was attributed to the significant fraction of barely passing ions which have a large effective orbit width, and thus strongly influence sawtooth behaviour [70, 71, 152].

Experiments in MAST [76] and TEXTOR [153] also exhibited an asymmetry in the sawtooth period when the injected NBI power was oriented either co- or counter-current, as shown in Fig. 4.13. In these smaller devices, the effect of rotation can become increasingly significant. Whilst the fast ions do have a stabilising influence, the large trapped fraction in spherical tokamaks is stabilising in either co- or counter-NBI regimes. On the other hand, the smaller moment of inertia and high beam power per unit volume in spherical tokamaks result in rotation speeds which approach the ion sound speed [72]. Such strong toroidal rotation results in sawtooth stabilisation, with the minimum in sawtooth period in the counter-NBI regime explained by relative direction of the flow induced by the NBI with respect to the intrinsic rotation of the plasma dominated by the ion diamagnetic drift [76, 154]. In TEXTOR, the sawtooth period reaches a minimum with a low level of co-NBI and a maximum in the counter-NBI regime [153]. This

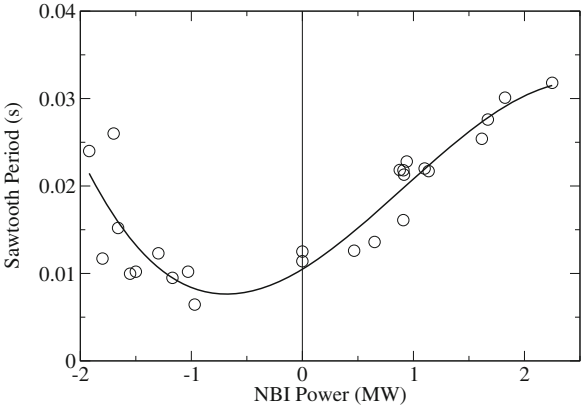

Fig. 4.13 Sawtooth period for MAST discharges as a function of applied NBI power. $I_P \in [680, 740]$ kA, $B_T \in [0.35, 0.45]$ T and $n_e \in [1.6, 2.3] \times 10^{20}$ m^{-3}. Negative beam power is taken to represent NBI power in the counter-I_P direction. Reproduced with permission from "The effect of toroidal plasma rotation on sawteeth in MAST" [74]

is due to a competition between the gyroscopic stabilisation of the kink mode and the destabilisation arising in the presence of counter-passing fast ions.

Numerical modelling to assess the effect on the $n = m = 1$ kink mode from both NBI-induced torques and from the resultant fast ion population considered the role played by on-axis co-NBI fast ions in lengthening the sawtooth period in JET. By assessing each of the triggering criteria given in 4.6–4.8 using the PRETOR transport code, Angioni et al. [99] predicted the nonlinear evolution of the sawtooth cycle with good agreement with empirical observations. Furthermore, the assessment of the kinetic effects has improved by applying drift kinetic codes including finite orbit width effects—for instance the Monte-Carlo guiding centre HAGIS code [155] has been applied to JET [40, 151]. Finally, the effect of toroidal rotation on the stability of the internal kink mode has also been assessed numerically [78, 154] and found to be important in determining sawtooth behaviour in fast rotating spherical tokamak plasmas [76].

Following the verification of the importance of passing fast ions in determining sawtooth stability and the observation that different NBI tangency radii led to different sawtooth behaviour [114], experiments were conducted to test whether off-axis co-NBI could be used to deliberately shorten the sawtooth period. The application of off-axis NBI such that the peak of the fast ion population was deposited outside the $q = 1$ surface did indeed result in a destabilisation of sawteeth in JET [156]. Furthermore, sawtooth control using off-axis NBI was also demonstrated in the presence of a concurrent stabilising fast ion population in the plasma core [157]. Figure 4.14 shows that additional off-axis NBI power in JET results in a decrease of the sawtooth period by a factor of three compared to the on-axis NBI only phase, despite an overall increase in β_h leading to stronger stabilisation from the trapped ions. Numerical modelling (also shown in Fig. 4.14)

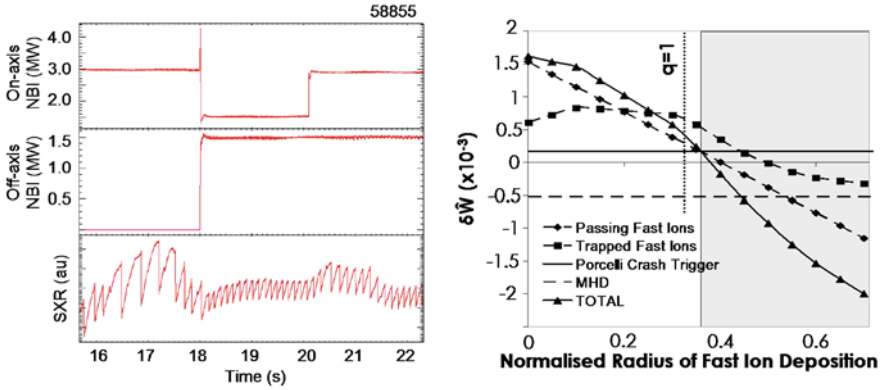

Fig. 4.14 (*left*) The soft X-ray emission and beam heating waveforms for JET shot 58855. The sawtooth period is significantly shorter when the total β_h is kept constant, but some off-axis NBI is used in place of on-axis heating. Further, this discharge also shows that the application of ancillary off-axis NBI can decrease the sawtooth period, despite an overall increase in β_h. Reproduced with permission from "Sawtooth control and the interaction of energetic particles" [157]. (*right*) The potential energy of the internal kink mode as a function of the deposition location of the centre of the fast ion population. When the fast ions are centred just outside the $q = 1$ surface, they destabilise the kink mode and consequently trigger sawteeth more frequently. Equations 4.6–4.9 suggest that a sawtooth crash will occur within the shaded region. Chapman et al. [156] published by Institute of Physics Publishing

confirmed that the passing fast ion effects dominantly determine the sawtooth behaviour.

Confirmation of the dominance of passing fast ion effects came from MAST and ASDEX Upgrade experiments which altered the radial gradient of the fast ion pressure at the $q = 1$ surface, and so changed the destabilising effect. In MAST this was achieved by displacing the plasma vertically such that the beam deposition moves from inside $q = 1$ to well outside [158]. In ASDEX Upgrade, the trajectory of the most off-axis positive ion neutral injector (PINI) was varied in order to move the deposition location of the energetic ions whilst keeping the plasma conditions relatively unchanged. Figure 4.15 shows the beam trajectories for different off-axis PINI inclination and the corresponding sawtooth behaviour. The passing fast ions destabilised the kink mode when the beam deposition location is well outside the $q = 1$ surface. This means that off-axis NBI faces severe limitations as a sawtooth control mechanism since $q = 1$ must be very core localised and even then, the destabilisation from kinetic effects must overcome gyroscopic stabilisation resultant from the beam torque.

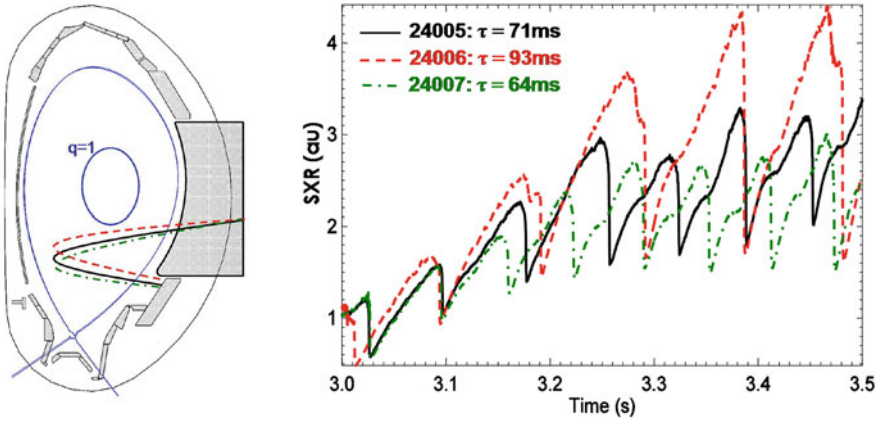

Fig. 4.15 (*left*) The beam trajectories of the off-axis PINI in ASDEX Upgrade as the PINI is tilted on its support. Also shown for comparison is the approximate position of the $q = 1$ surface, and (*right*) the corresponding soft X-ray emission in three ASDEX Upgrade plasmas. The sawtooth period decreases as the beam is injected further off-axis. Discharge 24006 represents the most on-axis NBI heating and shot 24007 is the most off-axis. Reproduced with permission from Chapman et al. [158] Copyright 2009, American Institute of Physics

4.5 Ion Cyclotron Resonance Heating

Early experiments with ICRH focussed on suppressing or delaying the first sawtooth crash, understood by the induced core fast ions stabilising the kink mode. On-axis ICRH was found to result in monster sawteeth, which often triggered NTMs [13, 159]. The long sawtooth periods and giant crashes were shown to be consistent with strong kinetic stabilisation through peaked fast ion pressures [49–51, 160] despite an increase in the destabilising fluid effects associated with the overall increase in pressure [161, 162]. This gave credence to the applicability of kinetic-fluid theory [47, 55] for modelling sawtooth behaviour in plasmas with ICRH. Soon after, experiments with off-axis heating showed that sawtooth destabilisation could also be achieved [113, 163]. Subsequently, control of sawteeth by ICCD has been widely exploited on JET [15, 42, 164–167], using two schemes, viz (i) minority ICCD where a minority ion species resonates with the fundamental cyclotron frequency of the ICRH wave, absorbing the RF power and carrying the fast ion current, and (ii) second harmonic ICCD, where an ion species (not necessarily a minority species) resonates at its second harmonic cyclotron frequency, $\omega = 2\omega_{ci}$ with the RF waves.

Whilst the stabilisation arising from on-axis ICRH was attributed to the trapped fast ion effects [58] and increase in fast ion pressure peaking [49], the destabilisation arising from off-axis ICRH was initially attributed to the non-inductively driven currents. The Fisch model [168] predicts that waves propagating in the co-current direction result in ICCD with a dipole structure with a positive part

(with respect to the plasma current) on the low-field side of the cyclotron resonance and a negative lobe on the high field side. For counter-propagating waves, the currents in the dipole structure change sign. This mechanism is reviewed succinctly in [113] and [166]. This classical model does not include finite orbit width effects of the resonating ions, acceleration of ions by waves in the parallel velocity, or trapped ions, though numerical calculations capable of including such effects are necessary for accurate determination of the ICCD [70, 160, 166, 169–171].

Analogous to the first ECCD sawtooth control experiments outlined in Sect. 4.3, early ICRH destabilisation experiments employed field and current ramps to sweep the ICRH resonance location across the inversion radius. However, the change in s_1 resulting from the ICCD dipole current perturbation is complicated by the fact that the $q = 1$ surface is radially displaced as the ICRH resonance moves [166]. Figure 4.16 shows the sawtooth behaviour in JET as the resonance of co-propagating ICRH waves (+90° phasing of the ICRH antenna) and counter-propagating waves (−90°) are swept across the $q = 1$ radius. +90° ICCD results in a strong stabilisation as the resonance is just outside the inversion radius since the shear is reduced, and even more stabilisation as the ICRH moves inside $q = 1$ due to the increase in fast ion pressure. Conversely, the −90° ICCD results in marked destabilisation with the resonance just outside $q = 1$ before an increase in sawtooth period is observed when the ICRH is well inside $q = 1$ and the trapped

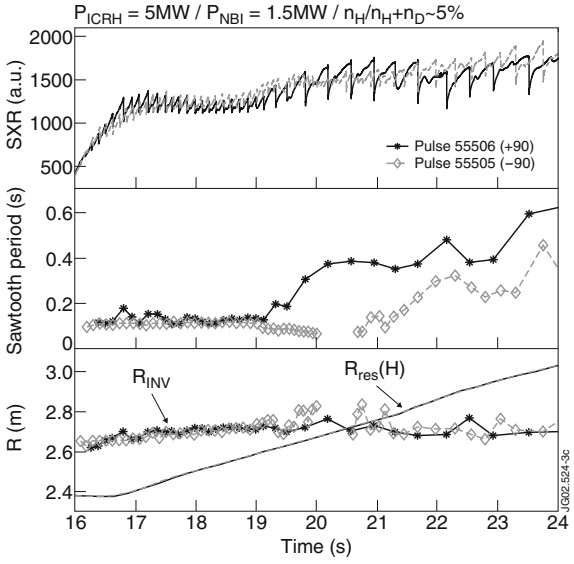

Fig. 4.16 The sawtooth behaviour during JET pules with co-propagating ICRH waves (+90°) and counter-propagating waves (−90°) as the resonance layer is moved across the inversion radius. The sawteeth are destabilised by the −90° ICCD just outside $q = 1$ before the increase in fast ions results in stabilisation when the resonance is well inside $q = 1$. The +90° waves are strongly stabilising when the resonance is both just outside and inside $q = 1$. Reproduced with permission from Mayoral et al. [42] Copyright 2004, American Institute of Physics

fast ion stabilisation begins to dominate. Note that ICRH wave induced pinch in the presence of an asymmetric distribution results in a more peaked fast ion pressure for co-moving waves [160], leading to the observed stronger stabilisation from on-axis heating.

It has also been demonstrated that ICRH is effective in keeping the sawtooth period short in the presence of a substantial core fast-ion population [165]. Figure 4.17 shows the sawtooth behaviour in JET where +90° ICRH is applied in the plasma core, resulting in fast-ion stabilised sawteeth, which are successfully destabilised by concurrent −90° ICCD near the $q = 1$ surface [165, 166]. Furthermore, ICCD control has also been demonstrated in plasmas with even more heating power on-axis from neutral beam injection and much higher β_p, well above the critical threshold for triggering of 3/2 NTMs in the absence of sawtooth control [172].

Detailed wave modelling showed that an ICRH resonance on the high field side gives optimised conditions for the classical Fisch model as the fast ion orbits are closer to the passing-trapped boundary. Conversely, a low field side ICRH resonance results in finite orbit width effects of trapped ions dominating the ICCD [169] decreasing in the magnetic shear near the resonance, independent of antenna phasing, as observed experimentally [167].

Whilst numerical modelling suggested that ICRH sawtooth control occurred primarily due to a change in local shear [113, 164, 166, 167], the sensitivity of sawtooth destabilisation required accuracy of the resonance position with respect to the $q = 1$ surface of less than 1 cm of the $q = 1$ surface in JET [172], which is far more sensitive than expected for control via current drive. Subsequently, Graves et al. showed that the sawtooth control mechanism responsible for localised off-axis toroidally propagating waves is due to the radial drift excursion of the energetic ions distributed asymmetrically in the velocity parallel to the magnetic

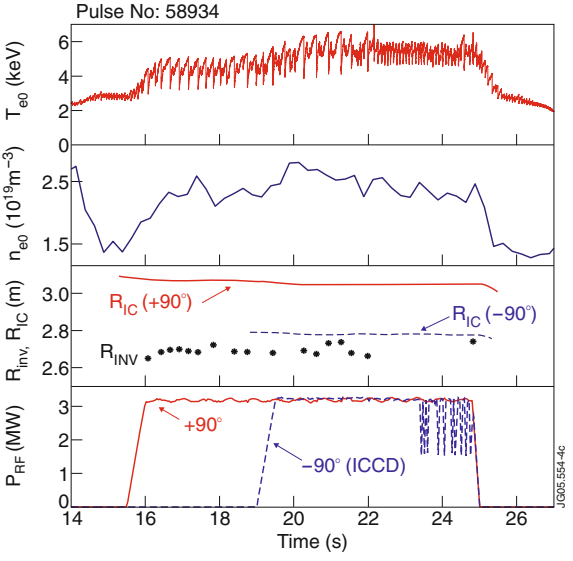

Fig. 4.17 The sawtooth behaviour during JET discharge 58934. When +90° ICRH is applied in the plasma centre the sawtooth period is significantly lengthened. Concurrent −90° ICCD near the $q = 1$ surface results in a destabilisation of the fast ion stabilised sawteeth. Reprinted figure with permission from Eriksson et al. [165]. Copyright 2004 by the American Physical Society

field [70]. Furthermore, this explains why ICRH is more effective than NBI for sawtooth control, since the orbit widths of the fast ions are larger and radial gradients of the parallel asymmetry of the fast ion distribution is stronger. The effect of asymmetry in the distribution was later simulated using SELFO [173] RF wave-field and fast ion distribution function simulations coupled with the drift kinetic HAGIS code, confirming the kinetic mechanism responsible for sawtooth control [152]. Finally, the kinetic mechanism also results in a deep and narrow minimum in the change of the potential energy when the peak of the passing fast ion distribution is just outside the $q = 1$ surface, explaining the extreme sensitivity of the sawtooth behaviour to the deposition location of the ICRH waves.

JET experiments were designed to differentiate between the fast ion and conventional current profile modification effects [70, 71] by using ^{3}He minority heating scheme is employed in a deuterium majority plasmas where the current dragged by the background plasma tends to cancel the ^{3}He current [113, 168, 174] resulting in negligible ICCD. Using such ^{3}He minority heating just outside the $q = 1$ surface led to a strong destabilisation for counter-propagating waves ($-90°$), overcoming the stabilisation from the core NBI-induced fast ions, and a strong stabilisation for co-propagating waves ($+90°$), as illustrated in Fig. 4.18.

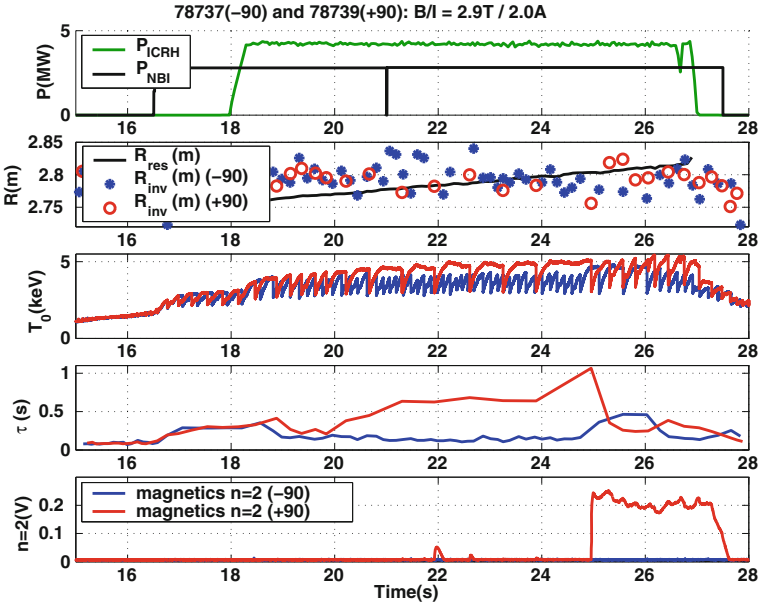

Fig. 4.18 JET pulses 78737 and 78739 with $-90°$ and $+90°$ ICRH off-axis respectively. The NBI fast ions in the core lead to long sawtooth periods. When the He^3 minority heating is deposited off-axis, the fast ions destabilise the sawteeth with $-90°$ phasing, but stabilise them with $+90°$ phasing, to the extent that a 1 s long sawtooth triggers an NTM. Reproduced with permission from "Experimental verification of sawtooth control by energetic particles in ion cyclotron resonance heated JET tokamak plasmas" [71]

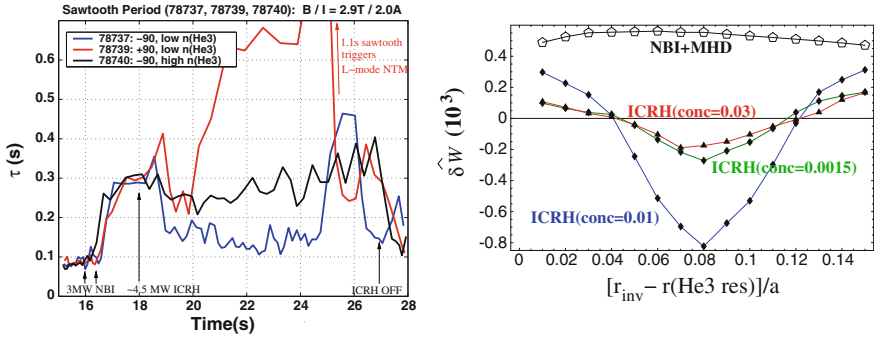

Fig. 4.19 (*left*) JET experiments showing that the fast ions due to He^3 ICRH heating just outside $q = 1$ (de)stabilise the sawteeth for $(-) + 90°$ phasing respectively for low He^3 concentration, but barely affect the sawtooth period at high concentration. This is replicated by drift kinetic modelling (*right*) which shows that the change in potential energy of the kink mode for trace concentration and for 3 % is negligible, whereas for 1 % concentration there is a strong and radially local effect. Reproduced with permission from "Experimental verification of sawtooth control by energetic particles in ion cyclotron resonance heated JET tokamak plasmas" [71]

For the $-90°$ phasing the sawtooth period is reduced to nearly the level of Ohmic sawteeth, whereas +90° increases the sawtooth period significantly, with the longest period of over 1 s triggering an $n = 2$ NTM. Further confirmation of this kinetic mechanism was attained by varying the concentration of the minority ions to change the amplitude of the fast ion mechanism. Figure 4.19 shows the sawtooth behaviour variation with minority ^{3}He concentration in three different JET discharges with $-90°$ phasing ICRH. For $n_{He}/n_e = 0.01$, the destabilising effect of the ICRH energetic passing ions dominates over the stabilising effect of the core NBI ions, with a commensurate reduction in sawtooth period. Conversely, at very low concentration ($n_{He}/n_e = 0.0015$) the minority power absorption is reduced and higher minority ion energies give rise to a broader fast ion distribution and enhanced losses, reducing the impact on sawtooth stability, whilst at high minority density, the reduced effective orbit width means that the effect of the ICRH ions is much smaller than the combined effect of NBI fast ions and fluid drive. This strong sensitivity to minority concentration is also seen in stability calculations shown in Fig. 4.19.

This means that toroidally-propagating ICRH waves could potentially be used for sawtooth control in ITER baseline scenario operation. Studies of the ion cyclotron current drive in ^{3}He minority schemes—as anticipated in ITER [10, 174]—predicted that drag currents will result in negligible driven current [113, 174], meaning that sawtooth control using ICCD was not envisaged for ITER. However, the recent development in understanding the effects of large orbit width passing fast ions near the passing-trapped boundary supported by experimental evidence using ^{3}He minority ICRH in JET, suggests that ICRH can be a useful tool for sawtooth control in ITER. The benefit of this mechanism is that it directly reduces the change in potential energy of the internal kink mode, meaning that a change in the magnetic shear due to concurrent current drive schemes is more

likely to destabilise the sawteeth successfully. However, since the resonance position of the ICRH must be so precisely localised with respect to the rational surface, real-time feedback is necessary for practical sawtooth control. Such real-time control through variation of the ICRH frequency has been attempted with some success on JET [175], though the frequency variation is much slower than anticipated in ITER.

4.6 Discussion and Implications for ITER

There has been considerable advancement in both the theoretical understanding and numerical prediction of sawtooth physics and the experimental techniques for sawtooth control, but there remain a number of open questions for sawtooth control in burning plasmas. Amongst these are: (i) What will the natural sawtooth period be in ITER?; and (ii) What is the maximum sawtooth period permissible without triggering an NTM? An early answer to the first question was proposed in [38] where the linear stability thresholds outlined in Sect. 4.2.3 were simulated using a 1–d transport solver, indicating a full reconnection sawtooth period of 100 s with a $q = 1$ radius of 50 % of the plasma minor radius. Subsequently, modelling using TSC [176] with profiles predicted by either the multi-mode model [177] or the Gyro-Landau fluid model GLF23 [178] predicted 50 s sawtooth period for full reconnection and 2–3 times shorter periods for partial reconnection, with a $q = 1$ radius of 42 % of the minor radius. This agrees well with the inversion radius predicted in BALDUR modelling [179]. Finally, time-dependent integrated predictive modelling with the PTRANSP code predicted a sawtooth period much less than 50 s [180]. There is therefore a large range in the predictions from 20 to 100 s, but perhaps more importantly, the issue of whether a sawtooth period in this range will avoid triggering NTMs is currently poorly understood. An empirical scaling of sawtooth-triggered NTMs in current devices provides a rudimentary answer [21], suggesting that at the target plasma pressure for baseline scenario operation, a sawtooth period in the range of 40–70 s will trigger an NTM.

Nonetheless, there have been developments in the capabilities and understanding of the actuators for sawtooth control in ITER even if the operational requirements to avoid NTMs is presently undefined. For instance, the electron cyclotron current drive profiles that can be expected from both the equatorial launcher and the upper launchers have been the subject of much investigation [181–184]. Ray-tracing calculations for the ECCD have allowed ASTRA simulations which include the effect of the fusion-born α particles according to [38, 96] to assess the sawtooth stability in ITER. This led to the prediction that a combination of 13.3 MW of co-ECCD from the equatorial launcher and 6.7 MW from the upper launcher would be able to reduce the sawtooth period by 30 %, or increase it by 50 % with a deposition inside or outside $q = 1$ respectively [185]. The fast ion distribution function arising from both on-axis and off-axis negative-ion neutral beam injection has also been computed [186] using the TRANSP code [187], and the effect of the

energetic ions on sawtooth stability has been computed [40, 185]. The N-NBI ions are found to be strongly stabilising to the internal kink, and can only incur destabilisation if the $q = 1$ radius is inside $r = 0.2a$. Finally, whilst numerical modelling of the ICCD expected using ^{3}He minority schemes in ITER predicts the maximum driven current density to be only 0.2–0.5 % of the plasma current density and insufficient for any significant modification to the magnetic shear profile [174], an assessment of the kinetic effects anticipated in ITER suggests that 10 MW of ICRH will be sufficient to negate the stabilising effects arising from the alpha population [185, 188]. Due to the inherent uncertainties in the numerical predictions, it is prudent that a combination of both ICRH and ECCD is planned for controlling sawteeth in ITER. In any case, it will be necessary to have real-time control of these actuators because of both the uncertainties in the control parameters (launcher aiming, ray-tracing, RF frequency) and the equilibrium (plasma position, q profile etc.) and the acute sensitivity of the radial location of the heating or current drive with respect to the rational surface, as highlighted in Sects. 4.3 and 4.5.

An alternative approach to controlling sawteeth is to deliberately maximise the sawtooth period. Indeed, this was originally considered the most desirable route to sawtooth amelioration in the original ITER Physics Basis [10], and was only superseded by destabilisation as anxiety grew about both the ramifications of triggering performance-degrading NTMs and the need for frequent expulsion of the on-axis accumulation of higher-Z impurities that would otherwise radiate energy. Long sawtooth periods are naturally achieved by applying early heating during the current ramp-up phase to increase the conductivity and so slow down the current penetration. Combining this with achieving early ignition will further stabilise the sawteeth due to the α particle stabilisation. ICRH could then be used as an ancillary control tool, with core heating providing a further population of strongly stabilising fast ions. Furthermore, in order to meet the $Q = 10$ goal of ITER baseline scenario, it is desirable to turn off the ECRH power whenever it is not being actively used for mode control. Thus, rather than being constantly required to modify the shear at $q = 1$, an alternative could be envisaged whereby fast ions are used to deliberately stabilise the sawteeth, and before each crash the ECCD is pre-emptively applied near the $q = 2$ surface to stabilise the ensuing NTM [137, 189, 190].

4.7 Summary

In burning plasmas, the significant energetic ion population is likely to result in long sawtooth periods, which in turn are predicted to increase the likelihood of triggering other confinement-degrading instabilities. Consequently, recent experiments have identified various methods to deliberately control sawtooth oscillations in an attempt to avoid seeding NTMs whilst retaining the benefits of small, frequent sawteeth, such as the prevention of core impurity accumulation. The primary methods used to achieve this are (i) tailoring the distribution of energetic

ions (ICRH or NBI); (ii) changing the radial profiles of the plasma current density and pressure, notably their local gradients near the $q = 1$ surface (ECCD, LHCD and to a lesser extent ICCD or NBCD); or (iii) heating the electrons inside the $q = 1$ surface (ECRH).

Energetic ions, plasma rotation and the local current density gradients can have a significant effect on the stability of the internal kink mode, thought to underlie the sawtooth phenomenon. Both trapped fast particles and passing fast ions with a large effective orbit width strongly influence sawtooth stability. Circulating ions affect the $n = m = 1$ kink mode through their radial drift excursion when distributed asymmetrically in the velocity parallel to the magnetic field. When these effects are combined, numerical modelling has been able to explicate the sawtooth behaviour observed with different heating and current drive actuators in a number of tokamaks. In order to destabilise the internal kink mode by tailoring the fast ion phase space, and so stimulate a sawtooth crash, the radial gradient of the passing fast ion distribution must be such that $\partial f_h(v_\parallel > 0)/\partial r > \partial f_h(v_\parallel < 0)/\partial r$, which occurs when the energetic ions are injected either off-axis ($\partial f_h/\partial r > 0$) and oriented with the plasma current, or when the fast ion population is predominantly on-axis ($\partial f_h/\partial r > 0$) and directed opposite to the plasma current.

When changing the plasma current density to control sawteeth, increasing the current just inside $q = 1$ increases s_1 and so destabilises the mode, whilst co-CD localised just outside $q = 1$ decreases s_1 and so stabilises the sawteeth. Conversely, driving counter-current just inside $q = 1$ results in stabilisation and just outside $q = 1$ gives rise to destabilisation. Destabilisation of sawteeth has been achieved using steerable electron cyclotron resonance heating which include real-time feedback schemes and robust sawtooth control despite the presence of energetic ions in the plasma core. Dramatic changes in sawtooth stability can also be achieved by the application of off-axis ICRH, both through changes to the magnetic shear, and perhaps dominantly, through establishing a strong radial gradient in the passing fast ion population just outside the $q = 1$ surface.

Whilst the present explanation of the physics of sawtooth oscillations remains incomplete, various robust control schemes have been established and are now well understood. Consequently, there is reasonable confidence that a strategy for sawtooth control in burning plasmas will be refined.

Glossary

I. Greek Symbols

β	Plasma beta, ratio of pressure to magnetic pressure, $\beta = 2\mu_0 p/B^2$
ϵ	Inverse aspect ratio, $\epsilon = r/R_0$
ϵ_1	Inverse aspect ratio of $q = 1$ surface, $\epsilon_1 = r_1/R_0$

η	Resistivity
γ	Linear growth rate
γ_{ad}	Adiabatic index, ratio of specific heats
Γ	Phase space
λ	Pitch angle, $\lambda = v_{\|}/v$
μ	Magnetic moment, $\mu = Mv_{\perp}^2/2B$
μ_0	Permeability
Φ	Scalar potential
Φ_{ad}	Third adiabatic invariant of motion
ϕ	Toroidal angle
$\dot{\phi}$	Toroidal precession frequency
$\rho_{i,e}$	Ion/Electron Larmor radius, $\rho_{i,e} = Mv_{\perp}/eB$
$\hat{\rho}$	Average Larmor radius, $\hat{\rho} = \sqrt{\rho_i^2 + \rho_e^2}$
ψ_t	Toroidal flux
ψ_p	Poloidal flux
ψ	Radial coordinate in toroidal geometry
ψ_*	Helical flux
ψ_1	Flux at the $q = 1$ surface
θ	Poloidal angle
ω	Mode frequency
$\tilde{\omega}$	Doppler shifted mode frequency, $\tilde{\omega} = \omega - \Omega_{\phi}(r_1)$
ω_b	Bounce frequency, $\omega_b = 2\pi/\tau_b$
ω_c	Cyclotron frequency, $\omega_c = eB/M$
ω_A	Toroidal Alfve'n frequency, $\omega_A = v_A/R_0$
ω_{*i}	Diamagnetic frequency of thermal plasma ions, $\omega_{*i} = (T_i dp_i/dr)/(eBp_i r_1)$
ω_{*h}	Diamagnetic frequency of hot ions, $\omega_{*h} = (\partial f_h/\partial P_{\phi}^0)/(\partial f_h/\partial \mathcal{E}^0)$
ω_{dh}	Drift frequency of hot ions, $\omega_{dh} \approx cE_h/4eBR_o r_1$
$\langle\omega_{dh}\rangle$	Bounce averaged magnetic drift frequency of hot ions
Ω_{ϕ}	Toroidal plasma rotation

Ω_E	Toroidal plasma rotation caused by electric potential, $\Omega_E = q\Phi^{'}/rB_0$
$\Delta\Omega$	Flow shear, $\Delta\Omega = \Omega_E(r) - \Omega_E(r_1)$
ξ	Fluid displacement
ξ_0	Fluid displacement at the magnetic axis
ξ_1	Fluid displacement at the $q = 1$ surface
ξ_a	Fluid displacement at the plasma edge
τ_A	Alfve'n time, $\tau_A = \sqrt{3R}/v_A$
τ_s	Sawtooth period
τ_E	Energy confinement time
τ_η	Resistive diffusion time
χ	Pitch angle, $\chi = v_\perp^2 B_0/v^2 B$
ζ	Toroidal coordinate, $\zeta = q\theta - \phi$
$\dot{\zeta}$	Toroidal precession frequency

II. Roman Symbols

a	Minor radius of the plasma edge
$\mathbf{A}$	Vector potential
B_ϕ	Toroidal magnetic field strength
B_θ	Poloidal magnetic field strength
$\mathbf{B}$	Magnetic field
e	Charge of particle
$\mathbf{E}$	Electric field
$\mathcal{E}_i$	Energy of ith particle
f_h	Hot minority ion distribution function
f_i	Thermal ion distribution function
f_0	Initial distribution function
$\delta f_{h,i}$	Perturbed hot or thermal ion distribution function
δf_{hk}	Perturbed fast ion distribution function due to kinetic effects
δf_{hf}	Perturbed fast ion distribution function due to fluid effects
$\mathbf{j}$	Current density

$\mathbf{k}$	Wave vector
m	Poloidal mode number
M	Particle mass
n_e	Electron number density
n_i	Ion number density
n	Toroidal mode number
p	Plasma pressure
$P_{\zeta,\phi}$	Canonical angular momentum
q	Safety factor, $q = 1/2\pi \int B_\phi / RB_\theta \mathrm{d}s$
R	Major radius
R_0	Major radius at magnetic axis
r	Minor radius
r_1	Minor radius at $q = 1$ surface
s	Magnetic shear, $S = r/qdq/dr$
s_1	Magnetic shear at $q = 1$ surface
T_i	Temperature of ions
T_e	Temperature of electrons
v_A	Alfve'n speed, $v_A = B_0/\sqrt{\mu_0 \rho_0}$
$\mathbf{v}_h$	Fast particle velocity
v_ϕ	Toroidal speed of plasma
$\mathbf{v}$	Particle velocity
$\mathbf{v}_{\|\|}$	Particle velocity parallel to the magnetic field
$\mathbf{v}_\perp$	Particle velocity perpendicular to the magnetic field

III. Potential Energy Terms

δW	Perturbed potential energy
δW_{MHD}	Perturbed potential energy due to MHD terms only
δW_{KO}	Perturbed potential energy due to collisionless thermal ions
δW_{core}	$\delta W_{core} = \delta W_{MHD} + \delta W_{KO}$
δW_h	Perturbed potential energy due to collisionless energetic ions

δW_{hf}	Perturbed potential energy due to hot ion adiabatic terms only
δW_{hk}	Perturbed potential energy due to hot ion non-adiabatic terms only
δW^t	Perturbed potential energy due to trapped hot ions only
δW^p	Perturbed potential energy due to passing hot ions only
$\hat{\delta} W$	Potential energy normalised as per [61], $\hat{\delta} W = \mu_0 \delta W / 6\pi^2 \xi_0^2 \varepsilon_1^4 R_0 B^2$

References

1. R.J. Hastie, Astrophys. Space Sci. **256**, 177 (1998)
2. J. Wesson, in *Tokamaks* (Oxford Science, Oxford, 1997)
3. J.P. Friedberg, in *Ideal Magnetohydrodynamics* (Plenum Press, New York, 1987)
4. S. Von Goeler, W. Stodiek, N. Sauthoff, Phys. Rev. Lett. **33**, 1201 (1974)
5. D.J. Campbell et al., Nucl. Fusion **26**, 1085 (1986)
6. Y. Nagayama et al., Nucl. Fusion **36**, 521 (1996)
7. H.K. Park et al., Phys. Rev. Lett. **96**, 195003 (2006)
8. H.K. Park et al., Phys. Rev. Lett. **96**, 195004 (2006)
9. I. Furno et al., Nucl. Fusion **41**, 403 (2001)
10. ITER Physics Basis, Nucl. Fusion **47**, S1 (2007)
11. M.F.F. Nave et al., Nucl. Fusion **43**, 1204 (2003)
12. M.F.F. Nave et al., Nucl. Fusion **35**, 409 (1995)
13. D.J. Campbell et al., Phys. Rev. Lett. **60**, 2148 (1988)
14. R.J. La Haye et al, in *Proceedings of 24th Europe Conference on Berchtesgarden*, vol. 21A Part III (European Physical Society, Geneva, 1997), pp. 1121–1244
15. O. Sauter et al., Phys. Rev. Lett. **88**, 105001 (2002)
16. A. Gude, S. Günter, M. Maraschek, H. Zohm, Nucl. Fusion **42**, 833 (2002)
17. R.J. Buttery et al., Nucl. Fusion **44**, 678 (2004)
18. R.J. Buttery et al, in *20th IAEA Fusion Energy Conference, Villamoura* EX/7-1 (2004)
19. R.J. Buttery et al., Nucl. Fusion **43**, 69 (2003)
20. E. Westerhof et al, in *Proceedings of 14th Joint Workshop on Electron Cyclotron Emission and Electron Cyclotron Heating* (Heliotopos Conferences Ltd, Santorini, 2006) p. 38
21. I.T. Chapman et al., Nucl. Fusion **50**, 102001 (2010)
22. R. Carrera, R.D. Hazeltine, M. Kotschenreuther, Phys. Fluids **29**, 899 (1986)
23. Z. Chang et al., Phys. Rev. Lett. **74**, 4663 (1995)
24. R.J. La Haye, Phys. Plasmas **13**, 055501 (2006)
25. O. Sauter et al., Phys. Plasmas **4**, 1654 (1997)
26. H. Zohm, Phys. Plasmas **8**, 2009 (2001)
27. D.P. Brennan et al., Phys. Plasmas **10**, 1643 (2003)
28. R. Fitzpatrick et al., Phys. Plasmas **2**, 825 (1995)
29. H.R. Wilson et al., Phys. Plasmas **3**, 248 (1996)
30. A.I. Smolyakov, A. Hirose, E. Lazzaro, G.B. Re, J.D. Callen, Phys. Plasmas **2**, 1581 (1995)
31. M. Kotschenreuther, R.D. Hazeltine, P.J. Morrison, Phys. Fluids **28**, 294 (1985)
32. H. Lütjens, J.F. Luciani, X. Garbet, Phys. Plasmas **8**, 4267 (2001)
33. C.C. Hegna, J.D. Callen, R.J. La Haye, Phys. Plasmas **6**, 130 (1999)
34. M.F.F. Nave et al., Nucl. Fusion **43**, 179 (2003)
35. H. Reimerdes et al., Phys. Rev. Lett. **88**, 105005 (2002)
36. P. Maget et al., Plasma Phys Control Fusion **47**, 357 (2005)
37. H.R. Koslowski et al., Nucl. Fusion **40**, 821 (2000)

38. F. Porcelli, D. Boucher, M. Rosenbluth, Plasma Phys. Control. Fusion **38**, 2163 (1996)
39. B. Hu, R. Betti, J. Manickam, Phys. Plasmas **13**, 112505 (2006)
40. I.T. Chapman et al., Plasma Phys. Control. Fusion **49**, B385 (2007)
41. M.J. Mantsinen et al., Phys. Rev. Lett. **88**, 105002 (2002)
42. M.L. Mayoral et al., Phys. Plasmas **11**, 2607 (2004)
43. R.J. Hastie et al., Phys. Fluids **30**, 1756 (1987)
44. J. Jacquinot et al., Plasma Phys. Control. Nucl. Fus. Res. **1**, 449 (1986)
45. D. Start et al, in *Proc 29th Annual Meeting of APS Division of Plasma Physics*, vol. 159 (San Diego, 1987) p. 286
46. M.F.F. Nave et al., Nucl. Fusion **42**, 281 (2002)
47. L. Chen, R.B. White, M.N. Rosenbluth, Phys. Rev. Lett. **52**, 1122 (1984)
48. K. McGuire et al., Phys. Rev. Lett. **50**, 891 (1983)
49. R.B. White, P. Rutherford, P. Colestock, M. Bussac, Phys. Rev. Lett. **60**, 2038 (1988)
50. R.B. White, M. Bussac, F. Romanelli, Phys. Rev. Lett. **62**, 539 (1989)
51. B. Coppi et al., Phys. Rev. Lett. **63**, 2733 (1989)
52. M.N. Bussac et al., Phys. Rev. Lett. **35**, 1638 (1975)
53. A. Martynov, J.P. Graves, O. Sauter, Plasma Phys. Control. Fusion **47**, 1743 (2005)
54. M. Kruskal, C. Oberman, Phys. Fluids **1**, 275 (1958)
55. T. Antonsen, B. Lane, J. Ramos, Phys. Fluids **24**, 1465 (1981)
56. G. Fogaccia, F. Romanelli, Phys. Plasmas **2**, 227 (1995)
57. R.J. Hastie, T.C. Hender, Nucl. Fusion **28**, 585 (1988)
58. F. Porcelli, Plasma Phys. Control. Fusion **33**, 1601 (1991)
59. J. Van Dam, M. Rosenbluth, Y. Lee, Phys. Fluids **25**, 1349 (1982)
60. T. Northrop, E. Teller, Phys. Rev. **117**, 215 (1960)
61. B. Briezman, J. Candy, F. Porcelli, H. Berk, Phys. Plasmas **5**, 2326 (1998)
62. F. Porcelli, R. Stankiewicz, W. Kerner, H. Berk, Phys. Plasmas **1**, 470 (1994)
63. J.P. Graves, O. Sauter, N. Gorelenkov, Phys. Plasmas **10**, 1034 (2003)
64. F. Porcelli et al, in *15th EPS Conference on Control. Fusion and Plasma Heating, Dubrovnik* **12B/1** 377 (1990)
65. J.P. Graves, R.J. Hastie, K.I. Hopcraft, Plasma Phys. Control. Fusion **42**, 1049 (2000)
66. J.P. Graves, Phys. Plasmas **12**, 090908 (2005)
67. S. Wang, T. Ozeki, K. Tobita, Phys. Rev. Lett. **88**, 105004 (2002)
68. J.P. Graves, Phys. Rev. Lett. **92**, 185003 (2004)
69. K. Ya, V.S. Marchenko, R.B. White, Phys. Plasmas **12**, 022501 (2005)
70. J.P. Graves, I.T. Chapman, S. Coda, T. Johnson, M. Lennholm, Phys. Plasmas **17**, 056118 (2010)
71. J.P. Graves et al., Nucl. Fusion **50**, 052002 (2010)
72. R.J. Akers et al., Nucl. Fusion **42**, 122 (2002)
73. F.L. Waelbroeck, Phys. Plasmas **3**, 1047 (1996)
74. C. Wahlberg, A. Bondeson, Phys. Plasmas **7**, 923 (2000)
75. R. Kleva, P. Guzdar, Phys. Plasmas **9**, 3013 (2002)
76. I.T. Chapman, T.C. Hender, S. Saarelma, S.E. Sharapov, R.J. Akers, N.J. Conway, Nucl. Fusion **46**, 1009 (2006)
77. C. Wahlberg, I.T. Chapman, J.P. Graves, Phys. Plasmas **16**, 112512 (2009)
78. I.T. Chapman, J.P. Graves, C. Wahlberg, Nucl. Fusion **50**, 025018 (2010)
79. S. Migliuolo, Nucl. Fusion **33**, 1721 (1993)
80. I.T. Chapman, Plasma Phys. Control Fusion 53, 013001 (2001)
81. ITER Physics Basis, Nucl. Fusion **39**, 2137 (1999)
82. B.B. Kadomtsev, Sov. J. Plasma Phys. **1**, 389 (1976)
83. M.N. Bussac, D. Edery, R. Pellat, J.L. Soule, *Plasma Phys. Controlled Nucl. Fusion Res.* (IAEA Vienna) **1**, 607 (1976)
84. G. Ara et al., Ann. Phys. **112**, 443 (1978)
85. S. Migliuolo, F. Pegoraro, F. Porcelli, Phys. Fluids B **3**, 1338 (1991)
86. M. Ottaviani, F. Porcelli, Phys. Rev. Lett. **71**, 3802 (1993)

87. A.J. Lichtenberg, K. Itoh, S.I. Itoh, A. Fukayama, Nucl. Fusion **32**, 495 (1992)
88. V. Igochine, O. Dumbrajs, H. Zohm, A. Flaws, Nucl. Fusion **47**, 23 (2007)
89. J. Wesson et al., Plasma Phys. Control. Fusion **28**, 243 (1986)
90. Y. Nagayama et al., Phys. Plasmas **3**, 1647 (1996)
91. T. Munsat et al., Nucl. Fusion **47**, L31 (2007)
92. C.G. Gimblett, R.J. Hastie, Plasma Phys. Control. Fusion **36**, 1439 (1994)
93. M.N. Bussac, R. Pellat, J.L. Soule, M. Tagger, Phys. Lett. **105A**, 51 (1984)
94. M.N. Bussac, R. Pellat, Phys. Rev. Lett. **59**, 2650 (1987)
95. Y. Nishimura, J.D. Callen, C.C. Hegna, Phys. Plasmas **6**, 4685 (1999)
96. T.K. Chu, Nucl. Fusion **28**, 1109 (1988)
97. G. Bateman, C.N. Nguyen, A.H. Kritz, F. Porcelli, Phys. Plasmas **13**, 072505 (2006)
98. O. Sauter et al, in *Theory of Fusion Plasmas, Proceedings of Joint Varenna-Lausanne International Workshop, Varenna* (AIP) p. 403 (1998)
99. C. Angioni et al., Plasma Phys. Control. Fusion **44**, 205 (2002)
100. C. Angioni, T. Goodman, M. Henderson, O. Sauter, Nucl. Fusion **43**, 455 (2003)
101. M. Choi et al., Phys. Plasmas **14**, 112517 (2007)
102. F.M. Levinton et al., Phys. Rev. Lett. **72**, 2895 (1994)
103. F. Porcelli, Phys. Rev. Lett. **66**, 425 (1991)
104. J.P. Graves et al., Nat. Commun. **3**, 624 (2012)
105. G. Bobrovskii et al., Sov. J. Plasma Phys. **13**, 665 (1987)
106. B.N. Kuvshinov, P.V. Savrukhin, Sov. J. Plasma Phys. **16**, 353 (1990)
107. K. Hanada et al., Phys. Rev. Lett. **66**, 1974 (1991)
108. R.T. Snider et al., Phys. Fluids B **1**, 404 (1989)
109. K. Hanada et al., Phys. Fluids B **4**, 2675 (1992)
110. E. Westerhof et al., Nucl. Fusion **43**, 1371 (2003)
111. Y. Ikeda et al., Nucl. Fusion **42**, 375 (2002)
112. A. Muck et al, in *29th EPS Conference on Controlled Fusion and Plasma Physics, Montreux,* vol. 26B, P1.037 (2002)
113. V.P. Bhatnagar et al., Nucl. Fusion **34**, 1579 (1994)
114. A. Mück, T.P. Goodman, M. Maraschek, G. Pereverez, F. Ryter, H. Zohm, Plasma Phys. Control Fusion **47**, 1633 (2005)
115. R.I. Pinsker et al., Bull. Am. Phys. Soc. **48**, 128 (2003)
116. A. Manini et al, in *32nd EPS Conference on Plasma Physics*, Tarragona, vol. **29C**, P4.073 (2005)
117. O. Sauter et al., Phys. Plasmas **8**, 2199 (2001)
118. M.A. Henderson et al., Fus. Eng. Des. **53**, 241 (2001)
119. H. Zohm et al., Nucl. Fusion **43**, 1570 (2003)
120. V.V. Ahkaev et al., Nucl. Fusion **35**, 369 (1995)
121. M. Maraschek et al., Nucl. Fusion **45**, 1369 (2005)
122. A. Manini et al, in *14th Joint Workshop on ECE and ECRH*, Santorini (2006)
123. T.P. Goodman et al., Nucl. Fusion **43**, 1619 (2003)
124. J.P. Graves et al., Plasma Phys. Control. Fusion **47**, B121 (2005)
125. A. Isayama et al., J. Plasma Fus. Res. Series **5**, 324 (2002)
126. M. Lennholm et al, in *17th Topical Conference on Radio Frequency Power in Plasmas*, vol. 933, p. 401 (2007)
127. M. Lennholm et al., Phys. Rev. Lett. **102**, 115004 (2009)
128. M. Lennholm et al., Fus. Sci. Tech. **55**, 45 (2009)
129. S. Cirant et al, in *17th IAEA Fusion Energy Conference,* Yokohama CDP/07 (1998)
130. M. Asakawa et al, in *17th IAEA Fusion Energy Conference,* Yokohama CDP/06 (1998)
131. Z.A. Pietrzyk et al., Nucl. Fusion **39**, 587 (1999)
132. H. Reimerdes et al., Plasma Phys. Control. Fusion **42**, 629 (2000)
133. A. Polevoi, S. Medvedev, V. Mukhovatov, A. Kukushkin, Y. Murakami, M. Shimada, A. Ivanov, ITER confinement and stability modelling. J. Plasma Fusion Res. **5**, 82–87 (2002)
134. J.I. Paley et al., Nucl. Fusion **49**, 085017 (2009)

135. J.I. Paley et al., Plasma Phys. Control. Fusion **51**, 055010 (2009)
136. J.I. Paley, F. Felici, S. Coda, T.P. Goodman, Plasma Phys. Control. Fusion **51**, 124041 (2009)
137. T.P. Goodman et al., Phys. Rev. Lett. **106**, 245002 (2011)
138. M. Lauret et al., Nucl. Fusion **52**, 062002 (2012)
139. G. Witvoet et al., Nucl. Fusion **51**, 103043 (2011)
140. V.G. Igochine et al, In prep for Nucl. Fusion (2010)
141. Y. Liu et al, *Private Communication* (2010)
142. I.T. Chapman et al., Nucl. Fusion **52**, 063006 (2012)
143. I.T. Chapman et al., Plasma Phys. Control. Fusion **55**, 065009 (2013)
144. A. Ekedahl et al., Nucl. Fusion **38**, 1397 (1998)
145. F.X. Söldner et al., Nucl. Fusion **34**, 985 (1994)
146. T.K. Chu et al., Nucl. Fusion **26**, 666 (1986)
147. S. Wukitch et al., Phys. Plasmas **12**, 056104 (2005)
148. A. Parisot et al., Plasma Phys. Control. Fusion **49**, 219 (2007)
149. G. Kramer et al., Nucl. Fusion **40**, 1383 (2000)
150. M.F.F. Nave et al., Phys. Plasmas **13**, 014503 (2006)
151. I.T. Chapman, S.D. Pinches, J.P. Graves, L.C. Appel, R.J. Hastie, T.C. Hender, S. Saarelma, S.E. Sharapov, I. Voitsekhovitch, Phys. Plasmas **14**, 070703 (2007)
152. J.P. Graves, I.T. Chapman, S. Coda, L.G. Eriksson, T. Johnson, Phys. Rev. Lett. **102**, 065005 (2009)
153. I.T. Chapman, S.D. Pinches, H.R. Koslowski, Y. Liang, A. Kramer-Flecken, M. de Bock, Nucl. Fusion **48**, 035004 (2008)
154. I.T. Chapman, G.T.A. Huysmans, A.B. Mikhailovskii, S.E. Sharapov, Phys. Plasmas **13**, 062511 (2006)
155. S.D. Pinches, L.C. Appel, J. Candy, S.E. Sharapov, H.L. Berk, D. Borba, B.N. Breizman, T.C. Hender, K.I. Hopcraft, G.T.A. Huysmans, W. Kerner, Comput. Phys. Commun. **111**, 133 (1998)
156. I.T. Chapman et al., Plasma Phys. Control. Fusion **50**, 045006 (2008)
157. I.T. Chapman et al., Nucl. Fusion **49**, 035006 (2009)
158. I.T. Chapman et al., Phys. Plasmas **16**, 072506 (2009)
159. C.K. Phillips et al., Phys. Fluids B **4**, 2155 (1992)
160. L.-G. Eriksson et al., Phys. Rev. Lett. **81**, 1231 (1998)
161. J.P. Graves et al., Phys. Rev. Lett. **84**, 1204 (2000)
162. K.G. McClements et al., Phys. Plasmas **3**, 2994 (1996)
163. D.F.H. Start et al, in *Proceedings of International Conference on Plasma Physics (Innsbruck)*, vol. 16C Part II (European Physical Society, Geneva, 1992) p. 1521
164. E. Westerhof et al., Nucl. Fusion **42**, 1324 (2002)
165. L.-G. Eriksson et al., Phys. Rev. Lett. **92**, 235004 (2004)
166. L.-G. Eriksson et al., Nucl. Fusion **46**, S951 (2006)
167. M. Mantsinen et al., Plasma Phys. Control. Fusion **44**, 1521 (2002)
168. N.J. Fisch, Rev. Mod. Phys. **59**, 175 (1987)
169. T. Hellsten, J. Carlsson, L.-G. Eriksson, Phys. Rev. Lett. **74**, 3612 (1995)
170. J. Carlsson, T. Hellsten, J. Hedin, Phys. Plasmas **5**, 2885 (1998)
171. M. Mantsinen et al., Phys. Rev. Lett. **89**, 115004 (2002)
172. S. Coda et al, in *Proceedings of 34th EPS Conference on Plasma Physics* (Warsaw, 2007) P5.130
173. J. Hedin et al., Nucl. Fusion **42**, 527 (2002)
174. M. Laxå back, T. Hellsten, Nucl. Fusion **45**, 1510 (2005)
175. M. Lennholm et al., Nucl. Fusion **51**, 073032 (2011)
176. S.C. Jardin, M.G. Bell, N. Pomphrey, Nucl. Fusion **33**, 371 (1993)
177. G. Bateman et al., Phys. Plasmas **5**, 2355 (1998)
178. R. Waltz et al., Phys. Plasmas **4**, 2482 (1997)
179. T. Onjun, Y. Pianroj, Nucl. Fusion **49**, 075003 (2009)

180. R.V. Budny et al., Nucl. Fusion **48**, 075005 (2008)
181. C. Zucca et al, in *Theory of Fusion Plasmas, Joint Varenna-Lausanne International Workshop, Varenna (AIP)*, vol. 1069, p. 361 (2008)
182. M. Henderson et al, in *3rd IAEA TM on ECRH Physics and Technology in ITER* (Como, 2005) p. 143
183. W.A. Houlberg et al., Nucl. Fusion **45**, 1309 (2005)
184. N.B. Maruschenko, H. Maassberg, Y. Turkin, Nucl. Fusion **48**, 054002 (2008)
185. I.T. Chapman et al., Nucl. Fusion **53**, 066001 (2013)
186. R.V. Budny, Nucl. Fusion **42**, 1383 (2002)
187. R.V. Budny et al., Nucl. Fusion **32**, 429 (1992)
188. I.T. Chapman et al., Plasma Phys. Controlled Fusion **53**, 124003 (2011)
189. O. Sauter, M.A. Henderson, G. Ramponi, H. Zohm, C. Zucca, Nucl. Fusion **52**, 025002 (2010)
190. F. Felici et al., Nucl. Fusion **52**, 074001 (2012)